NOVA SCHOOL OF SCIENCE & TECHNOLOGY

MATERIALS SCIENCE DEPARTAMENT

Gonçalo Miguel Rodrigues Catatão

BSc in Material Engineering Sciences

Additive Manufacturing and Characterization of Three-dimensional Anepectic Structures

MASTER IN MATERIALS ENGINEERING

NOVA University Lisbon

11, 2021

MATERIALS SCIENCE DEPARTAMENT

Additive Manufacturing and Characterization of Three-dimensional Anepectic Structures

Gonçalo Miguel Rodrigues Catatão

BSc in Materials Engineering Sciences

Adviser: Alexandre José da Costa Velhinho
Assistant Professor, NOVA University Lisbon

Co-advisers: João Paulo Miranda Ribeiro Borges
Associate Professor w/ Habilitation, NOVA University Lisbon

Examination Committee:

Chair: Professor Rui Jorge Cordeiro Silva,
Associate Professor, FCT-NOVA

Rapporteur: Maria de Fátima Reis Vaz,
Associate Professor, Instituto Superior Técnico of Universidade de Lisboa

Adviser: Alexandre José da Costa Velhinho,
Assistant Professor, FCT-NOVA

MASTER IN MATERIALS ENGINEERING

NOVA University Lisbon
11, 2021

Additive Manufacturing and Characterization of Three-dimensional Anepectic Structures

ACKNOWLEDGMENTS

Em primeiro lugar, gostaria de agradecer aos meus orientadores, Professor Doutor Alexandre Velhinho e Professor Doutor João Paulo Borges, por toda a ajuda e opinião fornecida ao longo deste trabalho. O constante contacto com eles foi de extrema importância para a realização da dissertação.

Agradeço a todos os docentes do DCM e ao CENIMAT que, não só tornaram a minha dissertação possível, como me formaram como engenheiro e me colocaram no caminho certo para me tornar num profissional de excelência. Um agradecimento especial ao João Cardoso que me ajudou em todos os passos da minha tese.

Um enorme agradecimento aos meus colegas do curso de Engenharia de Materiais por todos os momentos que passámos. Em especial agradeço ao Alvarez, Bento, Cabral, Duarte, Inês, Mónica, Rodrigo e Xue, por tornarem este percurso académico mais alegre e melhor.

Um agradecimento aos meus colegas Guilherme Cândida e Patrícia Almeida, por terem sido os meus colegas de dissertação. Agradeço pelo vosso companheirismo, as vossas ideias e por tornarem o tempo de laboratório mais divertido. Sem a vossa ajuda esta dissertação tinha ficado bastante diferente.

Um obrigado aos meus pais e irmão por me terem apoiado durante estes últimos 5 anos, pela vossa motivação. Sem vocês nada disto era possível. Um agradecimento ao resto da família, que apesar de estarem longe tiveram sempre presente.

Por último, mas não menos importante, agradeço à Rita. Foste a minha parceira durante a faculdade, obrigado pela paciência e por toda a ajuda que me prestaste. Foste um apoio fundamental para a realização desta dissertação.

ABSTRACT

In recent years there has been an increase of interest in 3D anepectic structures. An anepectic structure is a metamaterial with auxetic behaviour (Negative Poisson's Ratio (NPR)) and negative coefficient of thermal expansion (CTE). This work intends to manufacture and characterize a 3D anepectic structure using materials with positive CTE.

A known auxetic structure was used, in which a second material was incorporated to obtain a negative CTE. To achieve the design used in this work, mechanical and thermal finite element simulations were performed to preview the thermomechanical behaviour.

The 3D anepectic structures were produced by additive manufacturing using polyvinyl alcohol and Nylon. Two models with different designs were developed. Its characterization necessitated the development of new methodologies to determine the Poisson's ratio (PR) and CTE. One of the models obtained the intended anepectic behaviour. Furthermore, there was a correlation between PR values and the number of cells in the structure.

Until this day, this is the first published report of a manufactured and characterized 3D anepectic structure, making this work innovative in the area of metamaterials.

Keywords: Anepectic, Auxetic, Negative Coefficient of Thermal Expansion, Negative Poisson's Ratio, Additive Manufacturing, 3D Structures

RESUMO

Nos últimos anos tem existido um aumento de interesse em estruturas anepécticas 3D, isto é, auxéticas (Coeficiente de Poisson negativo (NPR)) e com coeficiente de expansão térmica (CTE) negativo. Este trabalho pretende manufaturar e caracterizar uma estrutura anepéctica 3D, constituída por materiais com CTE positivos.

Foi utilizado uma estrutura auxética conhecida, no qual se incorporou um segundo material com o intuito de obter um CTE negativo. Para obter esse *design*, realizou-se simulação mecânica e térmica de elementos finitos.

As estruturas anepécticas 3D foram produzidas por fabricação aditiva utilizando PVA e Nylon. Foi desenvolvido dois modelos com diferentes *design*s. Para a sua caraterização foi necessário desenvolver metodologias novas para a determinação do PR e do CTE. Sendo que um dos modelos obteve o comportamento anepéctico pretendido. Para além disso, verificou-se uma correlação entre os valores de PR e o número de células na estrutura.

Até à data, esta é a primeira publicação de uma estrutura anepéctica 3D manufaturada e caraterizada. Tornando este trabalho inovador na área dos metamateriais.

Palavras chave: Anepéctico, Auxético, Coeficiente de expansão térmica negativo, Coeficiente de Poisson negativo, Fabricação aditiva, Estruturas 3D

CONTENTS

LIST OF FIGURES

LIST OF TABLES

ACRONYMS

2D	Two dimensional.
3D	Three dimensional.
ABS	Acrylonitrile butadiene styrene
CLTE	Coefficient linear of thermal expansion
CTE	Coefficient of thermal expansion
DER	Double-Elliptic Ring
FFF	Fused filament fabrication
FE	Finite element
NPR	Negative Poisson's ratio
NTE	Negative thermal expansion
PPR	Positive Poisson's ratio
PR	Poisson's ratio
PVA	Polyvinyl alcohol

SYMBOLS

a, b, c	Inner radius of ellipse
L	Length
m	Form factor of the elliptic rings in the xy plane
min	Minute
mm	Milimeter
mm/s	Milimeter per second
MPa	Megapascal
N	Newton
n	Form factor of the elliptic rings in the yz plane
q	Thickness of the elliptic ring
T	Temperature
T_g	Glass transition temperature
t_0	Width of the elliptic rings
t_1	Width of the inner material
°	Degrees (angle)
°C	Degrees Celsius
α_L	Coefficient linear of thermal expansion in L direction
ε_L	Strain along the load direction
ε_T	Strain along the transverse direction

$\boldsymbol{\Phi}$	Angle between the center of the inner material and its edge
$\boldsymbol{\nu_{L,T}}$	Poisson's ratio

MOTIVATION AND OBJECTIVES

Over the past few years, there have been an increased interest in creating three-dimensional (3D) structures with a negative Poisson's ratio and negative coefficient of thermal expansion. Creating a structure that combines these two properties, called anepectic, has been taking its first steps. These structures could be relevant in biomaterial applications, aerospace, sensors, and composite materials. So far, the anepectic behavior of 3D structures has only been proven through analytical and finite element analysis.

Thus, based on the auxetic elliptic double ring structure, this dissertation aims to design, manufacture, and characterize mechanically and thermally the first non-virtual 3D anepectic structure. The main points of innovation are the design of a new anepectic structure and the experimental characterization of an anepectic 3D structure, proceeding to validation of behaviour through mechanical and thermal tests. To design the structure, finite element analysis will be performed, and for manufacturing the anepectic structure, it will be necessary to use additive manufacturing.

It is also intended to start understanding how the design parameters influence the thermal and mechanical behaviour of the structures.

1

INTRODUCTION

1.1 Metamaterial

The designation metamaterial, from Greek "μετα" (beyond) and the Latin "materia" (material), refers to a material whose properties come essentially from its structures and not its composition [1]–[3]. Due to their design, metamaterials can have properties that are unusual in conventional materials [2]–[5].

Bose developed the first metamaterial for optics applications, but since then, acoustic and mechanical metamaterials have also been developed [6], [7]. Mechanical metamaterials are a subclass that aims to achieve specific mechanical properties due to their structure geometry [2], [7].

The possibility of designing metamaterials with tailor made properties beyond the conventional material is desirable to optimize to the pretended application. These metamaterials are composed of conventional materials with typical values for these properties. Among the unusual ranges of properties obtained in metamaterials stand out: negative Poisson's ratio (NPR), negative thermal expansion (NTE), negative compressibility, among others [2]. Studies of combining two or more negative properties in the same metamaterial only emerge in the last decade [2].

1.2 Auxetics

The elastic constant Poisson's Ratio (PR, $\nu_{L,T}$) is defined by:

$$\nu_{L,T} = -{}^{\varepsilon_T}/_{\varepsilon_L} \tag{1.1}$$

where ε_L and ε_T are the strains along the load direction and the transverse direction, respectively [1], [8]. Conventional materials have a positive PR, which implies that, under

uniaxial compression, the material will expand along the orthogonal directions of the applied force, Figure 1.1 - a) [1], [9].

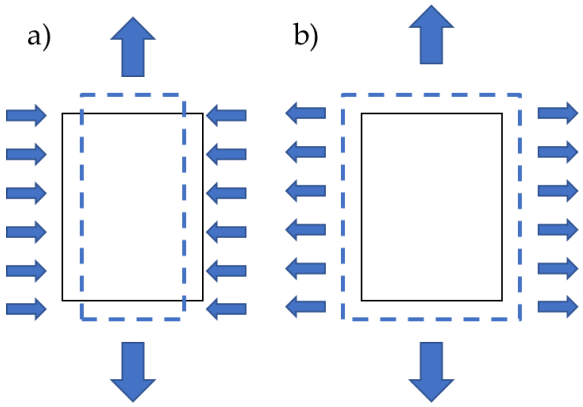

Figure 1.1 - a) Material with positive PR. b) Material with NPR.

A NPR structure is denominated auxetic and is characterized by shrinking (expanding) transversely when uniaxially compressed (tensioned), Figure 1.1 - b) [8], [10]. The geometry of the auxetic metamaterial is crucial to obtain this characteristic [11].

There are several naturally occurring structures that manage to reach a NPR; examples of this are some zeolites [12], [13], graphene monolayers [14], [15], and silicon dioxide [16], [17]. There is a high demand for artificial auxetic structures, both macro and micro scale. Among them, the following categories stands out: re-entrant models [18]–[20], double arrowhead [21]–[23], interconnected star models [3], [24], [25], models with rotating units [26]-[28] and ring-rod assembly [11], [29], [30]. The last structure will be studied in more detail throughout this dissertation.

Metamaterials with NPR are gaining interest in the biomedical industry. One of the most significant possibilities is their incorporation in stents [31], [32]. Dental floss [33] and smart bandages [34] are other applications in biomedicine. In addition, auxetic metamaterials have a wide range of applications: aerospace, military, sensors, filters, and textile industry [1], [10], [33], [35].

1.3 Coefficient of thermal expansion

Most solids have a positive coefficient of thermal expansion (CTE), i. e., expand upon raising the temperature [3], [9]. This phenomenon is due to the increase in the interatomic bond length as a result of the increased atomic and molecular vibrations [36], [37]. There are liquids and solids with NTE, usually associated with phase transformations, among them water [38], [39], some oxides [40]–[42], zeolites [43], [44] and some polymers [45], [46]. The mechanisms subjacent to this behaviour can be classified into three categories: flexible network, atomic radius contraction, and magnetovolume effect [47], [48].

It is possible to obtain metamaterials with NTE, although their constituents have positive CTE values. That is due to the geometry and the use of two materials with different positive CTE [49]–[51]. These structures can be classified as either bending-dominated structures whose walls bend and/or rotate due to concavities in the geometry, or to being bimaterial that will bend the walls or block; or, alternatively, as stretching-dominated structures, where the walls are made of two materials with different CTE in the form of triangles or tetrahedrons [4], [52], [53].

Materials may expand in isotropic or anisotropic form. In isotropic materials, the expansion occurs by the same extent in any direction. However, when the extent varies with the direction considered, the material is defined as anisotropic. For the last ones, the coefficient linear of thermal expansion (CLTE, α_L) is used and defined by:

$$\alpha_L = \frac{1}{L}\frac{\partial L}{\partial T} \tag{1.2}$$

where L is the length of the direction studied, and T is the temperature. [48], [54], [55]

The use of materials with NTE in composites allows them to act as thermal expansion compensators, making the composite a zero CTE. In addition they can reduce thermal stresses [47], [56], [57]. Metamaterials with NTE also have applications in the areas of electronics [48], aerospace [51], [55], civil engineering [55], and dental fillings [48], [56].

1.4 Anepectic

The anepectic designation, created by Raminhos et al. [58], applies to a material that simultaneously features NPR and NTE. Despite the scientific interest in recent years around this topic, the development of metamaterials with anepectic behavior is still beginning. [5]

Previous studies of anepectic structures focused primarily on two-dimensional (2D) structures, and most of these studies are finite element (FE) analysis and/or analytical analysis. The main 2D anepectic meshes studied until now are triangles connected [59], reentrant stars [3], [4], reentrant triangles [9], [60] and hybrid honeycomb [4], [61]. There are 2D meshes with experimental work: chiral [62] and stars reentrants [52], [58].

According to the literature, the first 3D metamaterial with anepectic properties was developed by Ai et al. [63]. The authors used FE method to demonstrate its anepectic properties. After Ai et al., between 2020 and 2021, more anepectic structures were designed and analyzed through modeling by FE and/or analytical analysis [50], [53], [64]–[69]. So far, none of these structures have carried out thermal and mechanical tests to validate their anepectic properties experimentally. Some of these structures are represented in Figure 1.2.

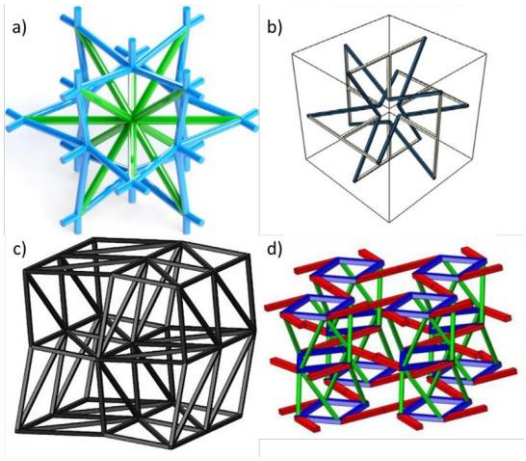

Figure 1.2 - Unit cell developed by Sarvestani et al. [67]; b) Unit cell re-entrant honeycomb by Peng et al. [66]; c) Structure design by Chen el al. [64]; d) Structure developed by Fu et al.[53].

One of the most discussed applications is dental filling, because the materials used for this purpose undergo a sudden temperature variation due to food and drink and must withstand the forces of chewing [53], [63]. Another application is in satellites, as these suffer variations greater than 200ºC between exposure and concealment from sunlight [9], [64]. Beyond that, it can be use in the aeronautic field [55]; antennas [53]; solar panels [53], [63], [64]; smart sensors [52], [60]; composite materials [52]; thermal and electrical components [52] and filters [63].

1.5 Double-Elliptic Ring (DER) structure

The design of an anepectic structure has been usually based on an auxetic structure, suitably modified to also acquire a NTE [3], [60]. The current work is based on a structure created by Wang et al., called latitude-and-longitude-inspired double-elliptic-ring structure (DER) [29]. The authors obtained a partially auxetic 3D metamaterial with the Poisson's ratio being positive in one direction and negative in the other.

The unit cell of the DER structure is composed of two orthogonally oriented ellipses, Figure 1.3 - a). When there is a compression in the z direction, the blue ellipse will expand in the x direction, i.e., points C and D will move apart. As a result, in the y direction, the green ring will contract, and points E and F will approach. This way, the unit cell has positive PR in the x direction and NPR in the y direction [29].

One of the structures studied by Wang et al. is represented in Figure 1.3 - b), obtained by replicating the unit cell on the three axes. The authors concluded that it exhibits a partially auxetic behavior through analytical analysis, FE analysis ,and mechanical tests [29], [70].

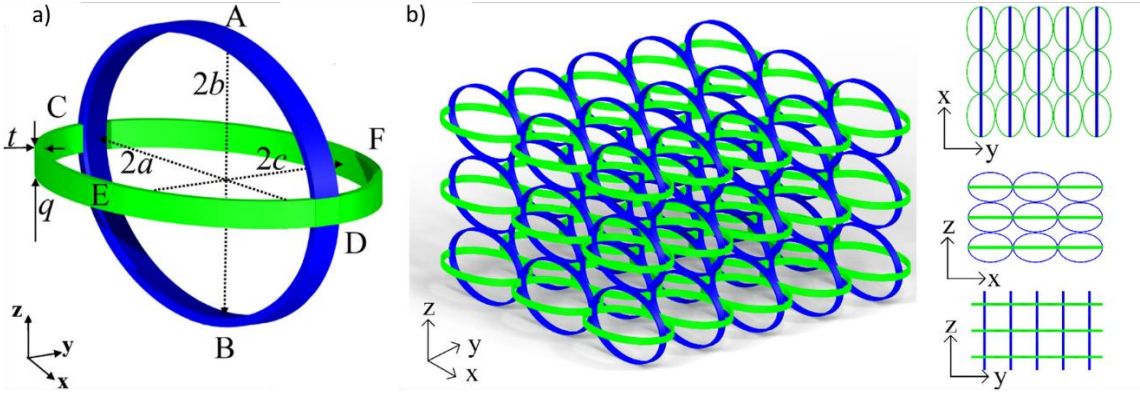

Figure 1.3 - a) Unit cell of DER structure adapted from Wang et al.; b) DERs partially auxetic.[29].

1.6 Research methodology

In the literature, it is common to use computer simulation to study the behaviour of possible anepectic structures [52], [63], [65]. The use of this technique through the FE method allows understanding the behaviour of these structures when applying forces or varying the temperature, as was done by Sarvestani et al. [67]. In addition, computer simulation software allows the design of the structures to simulate their behaviour and optimize their parameters.

Many of the methods of producing metamaterials are based on techniques of additive manufacturing due to the advantage of manufacturing complex geometries in a fast and cheaper way [10], [71], [72]. In addition, it can produce structures with a high number of different materials [10], [72]. The techniques of 3D printing can be summarized in the following steps: design of the model in modelling software, dividing the model into layers (slicing), and finally printing [71].

There are several 3D printing techniques, but the most predominant are stereolithography, selective laser sintering, and fused filament fabrication (FFF or FDM) [71]. The FFF technique will be used to produce the structures studied in this work. It consists of the extrusion of a plastic filament through a heated nozzle. This deposition is layer by layer [71], [72]. Several parameters will influence the final properties of the structure, namely: the nozzle diameter, the extrusion flow rate, deposition speed, extrusion temperature, filament brand, among others [72], [73].

This work aims to produce an anepectic 3D structure inspired by the DER and validate its properties through mechanical and thermal experiences.

2

MATERIALS AND METHODS

2.1 Structure design and printing equipment

The software used to model all the structures created in this work was SolidWorks 2020. A compromise between a reasonable printing time and the mitigation of boundary effects was achieved by selecting structures made from 3 x 3 x 3 unit cells for the majority of the experimental tests performed.

An Ultimaker 3™ 3D printer was used; this model uses a FFF technique and is capable of dual extrusion, with a nozzle diameter of 0.4 mm. All the prints had 100% infill to produce a solid structure, and the layer height was 0.15 mm. The slicer software used was Ultimaker Cura 4.8. After the print, all structures are stored in vacuum desiccators to prevent humidity absorption.

2.2 Finite element method

Thermal and mechanical behaviours were simulated through finite element method using SolidWorks 2020. A solid mesh type was used consisting of 8.925 mm tetrahedral mesh element size. For both mechanical and thermal simulations, a roller/slider in the yz, xz and xy plane, as shown in green in Figure 2.1, was used. For the mechanical simulation, a force of 10 N per item (pink arrows in Figure 2.1) was applied. For the thermal simulation, the temperature was raised from 0 ºC to 200 ºC.

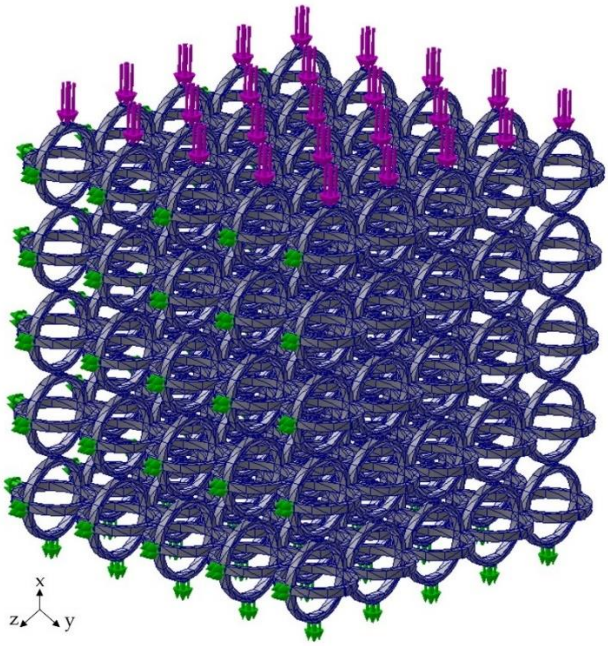

Figure 2.1 - Example of a mechanical simulation by finite element method.

2.3 Filament characterization

The filaments used to fabricate the different structures were polyamide (Nylon, PA6/66, Ultimaker) and polyvinyl alcohol (PVA, Ultimaker). For the mechanical characterization, both compression and tensile tests according to ASTM Standard D695-15 and ASTM Standard D638-14, respectively, were performed. All the test specimens were printed both vertically and horizontally, with no walls, 0.15 mm layer height and 100% infill. The compression tests were filmed with the intent of calculating the PR of the bulk materials from the recorded images.

2.4 Poisson's Ratio determination method

To determine the PR, the mechanical tests of the DER structures and the filament characterization were performed with a Shimadzu AG-50kNGT universal testing machine. All tests were performed at 1mm/min using a load cell of 50 kN. To determine $\nu_{z,x}$ and $\nu_{z,y}$ the experiments were filmed with two cameras simultaneously; one to film the xz plane (Galaxy S8 SM-G950F) and the other (Canon EOS 750D with 18-55mm lens) the yz plane. These cameras were set in parallel to the respective plane and centered to the middle cell. This was the best way to mitigate the parallax effect, although it was impossible to completely eliminate the effect due to the size of the structure.

To obtain the distances between reference points a primary spray was applied (Fine Surface Primer (L) for Plastic & Metal (White) from TAMIYA), then red nail polish (from

MyLabel) and matte effect (Matte Effect Top Coat from KIKO MILANO). The reason behind the application of the matte effect was the removal of the light reflection from the nail polish. This light reflection appears as white points in the videos changing the center points throughout all the experiments.

For the calculation of PR, a MATLAB code was developed that processes all the raw data obtained from the mechanical tests (videos, stroke, and force data). The output given by the code is the stress-strain curve and the PR throughout the test. The developed algorithm is presented in Appendix A with the corresponding explanation.

An example of the raw data obtained by the developed MATLAB code is depicted in Figure 2.2. Due to camera resolution limitations, a vast variation is observed at the beginning of the experiment. For that reason, the initial data has been discarded. Furthermore, the data displays noise throughout the trial on the right side of the figure. To reduce the noise, a binomial fit (usually, polynomial order five) was performed using the OriginPro 2018 software, with the x axis being the relative displacement and the y axis the average distance between points of the pretended direction. Afterwards, using the fitting distance equations, it becomes possible to determine the respective strains and, lastly, the PR using the equation (1.1), obtaining the final data corresponding to the red line of Figure 2.2.

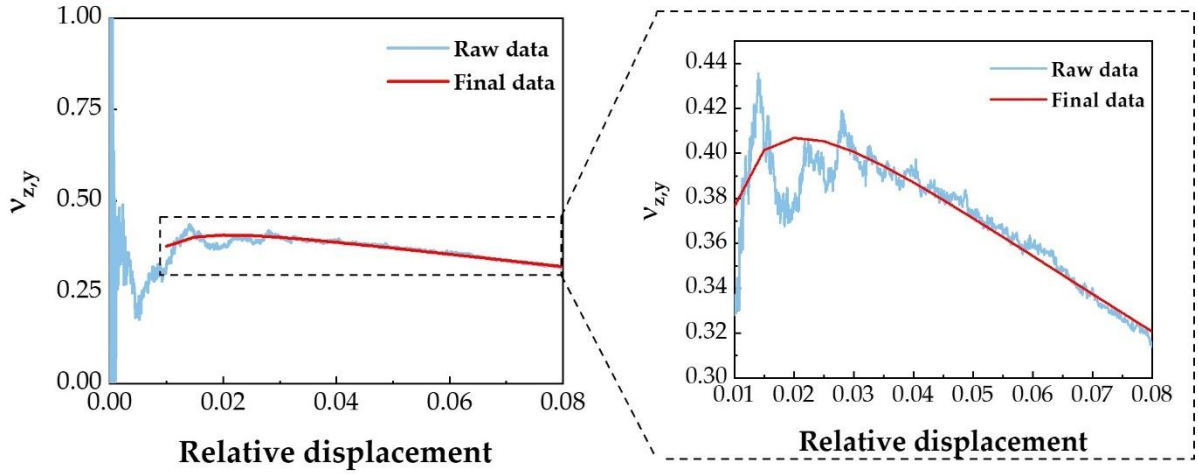

Figure 2.2 - Comparison between the PR of the raw data obtained by MATLAB code and applying a binomial fit of the distance data.

2.5 Coefficient of thermal expansion determination method

The set-up in Figure 2.3, with glycerol ($HOCH_2CH(OH)CH_2OH$, LABCHEM, 100%) in a transparent container with flat walls (to reduce image distortion) was used to determine the CTE of the structures. To register the temperatures throughout the experiment, three type-k thermocouples (Figure 2.3 - 6) were used, connected to a data logger (Pico TC-08 and PicoLog 6 Software) (Figure 2.3 - 1). Two smartphones (Galaxy S8 SM-G950F and Galaxy ACE SM-G358FX) were used to take pictures every minute, one to register the xz plane and the other the yz plane (Figure 2.3 - 2). To minimize parallax effect, the cameras were aligned with the middle cell.

Since the samples floated in glycerol, supports were produced to immobilize the structure. These supports were made of acrylonitrile butadiene styrene (ABS) because its T_g is above 90 ºC and the experience was limited to 80ºC [74]. Stainless steel wires were placed to not allow movement or rotation in any of the axes while trying to restrict the structure as little as possible (Figure 2.3 - 5).

The temperature during the experiment was increased from ambient temperature up to 80 ºC. A hot plate and a magnetic stirrer were used (Figure 2.3 - 3), to obtain the best temperature uniformity throughout the container during the test.

Before this experiment, similarly to the PR method, red dots were marked on strategic places, and an algorithm was created in MATLAB for the CTE calculations, which can be found in Appendix B.

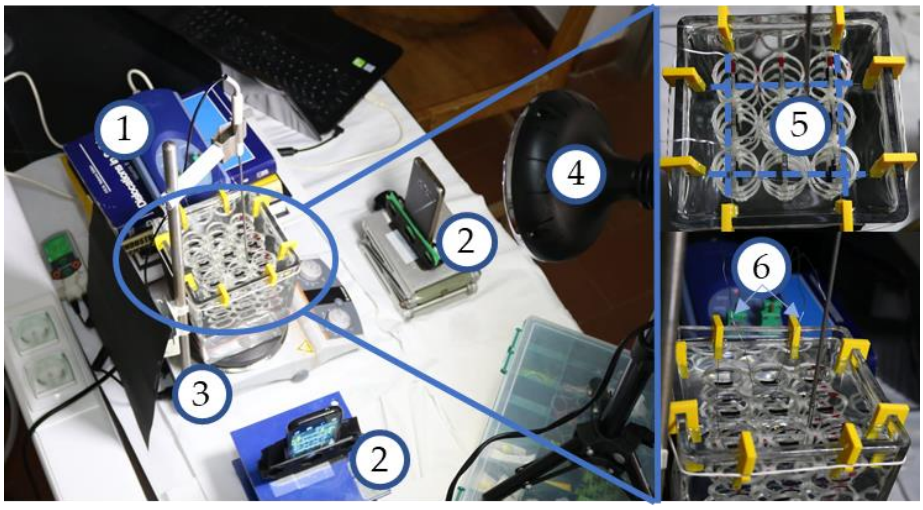

Figure 2.3 - Set-up of the thermal experience. 1: PicoLog 6; 2: Smartphones; 3: Heat plate; 4: Spotlight; 5: Stainless steel wires; 6: Thermocouples.

3

RESULTS AND DISCUSSION

3.1 Filament Characterization

The two materials chosen for the current work are Nylon and PVA since it was reported in previous works that their combinations could obtain the anepectic behaviour pretended. This is due to having a similar but different stiffness, and a distinct CTE. [49], [58], [75]

Mechanical tests were performed to obtain the mechanical properties of the filaments used, Nylon and PVA. Appropriate specimens were printed according to two different printing orientations (horizontal and vertical) to understand the relevance of the printing orientation. The average stress-strain curves of the tensile and compression tests are represented in Figure 3.1. All the stress-strain curves are represented in Appendix C.

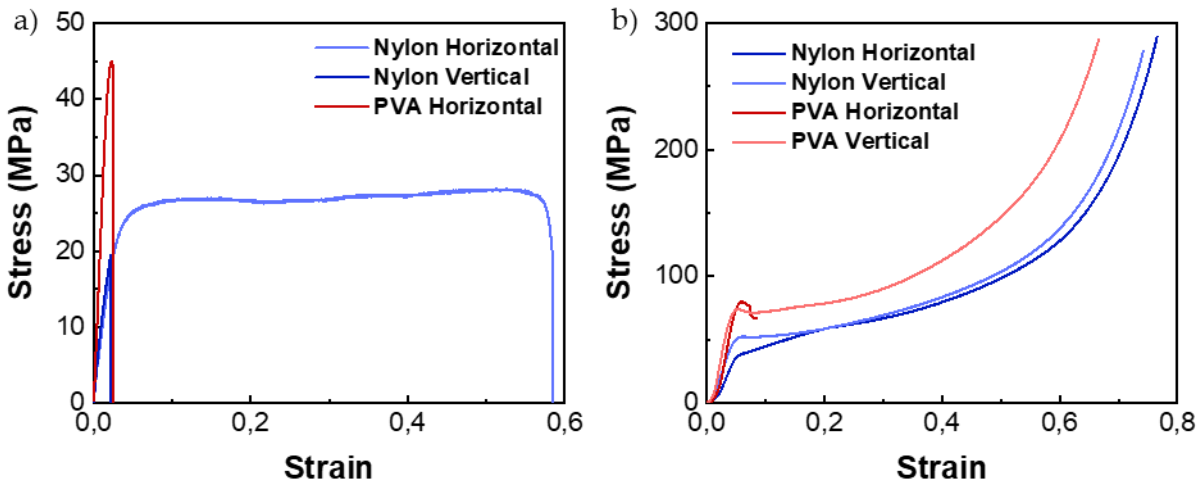

Figure 3.1 - Stress-strain curve of the sample average of Nylon and PVA in different orientations a) Tensile test b) Compressive test.

Table 3-1 shows the results of the Young's modulus, PR and fracture strain of the printed specimens. The three samples of PVA with vertical printing orientation fractured during installation on the testing machine, prior to the tensile test; this shows the fragile behaviour of these samples whenever printing vertically. That is due to a poor adhesion between layers when printing with the FFF technique. The Nylon samples present the same tendency, showing a ductile behaviour for the horizontal orientation and fragile behaviour for the vertical orientation prints.

Table 3-1 - Mechanical properties Nylon and PVA in horizontal and vertical printing directions.

		Young's Modulus (MPa)	**PR**	**Strain of fracture**
Nylon	Horizontal	784.49	0.34	0.555
	Vertical	855.82	0.30	0.022
PVA	Horizontal	2484.34	0.27	0.027
	Vertical	-	0.22	-

These results show the tremendous impact of the printing orientation on the mechanical behaviour of the samples due to the bad adhesion between layers.

The glass transition temperature (T_g) and the CTE of the Ultimaker Nylon and PVA filament have been determined by Raminhos et al. [58]. These results are presented in Table 3-2. It is essential to note out that these values may not be exact for this work because another batch was used, although the supplier is the same. Furthermore, based on the literature, the filaments of the same brand have values similar to those considered in this work [76], [77].

Table 3-2 - T_g and CTE of Nylon and PVA (obtained from Raminhos et al.) [58].

	T_g (ºC)	CTE ($\times 10^{-6}$ ºC^{-1})
Nylon	35	166.47
PVA	35	28.35

3.2 Structure design

3.2.1 Finite element analysis

To achieve the anepectic behaviour, some modifications to the DER structure were done. Parts of the structure were replaced with another material of higher CTE, with the intend of achieving a thermal expansion behaviour similar to the mechanical compression behaviour observed during mechanical testing by Wang et al. [29].

Four different cell arrangements were simulated through finite element (FE) method to predict the corresponding PR and CTE values; the characteristics of three of these arrangements are presented in Appendix D. The unit cell of Figure 3.2 was chosen as the object of study due to the exhibition of anepectic behaviour. It is observed that the unit cell of Figure 3.2 obtained a NTE in axis x and z due to the expansion of the nylon (in red).

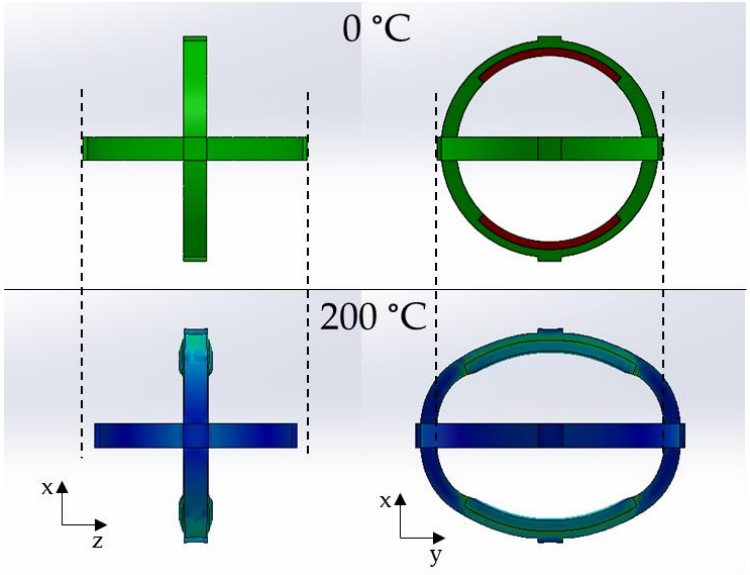

Figure 3.2 - Thermal expansion simulation of a cell, shows the NTE in x and z axis and positive CLTE in y axis.

The green material is PVA (lower CTE) while in red is the Nylon material. The design parameters used to obtain this cell was the same of the Wang et al [29] specimen S2, with the angle between the center of the inner material and its edge of 45 ^{o} and the inner material width of 1 mm.

3.2.2 Design parameters

Due to the anepectic behaviour previously predicted by the FE analysis, the unit cell shown in Figure 3.3 was chosen as the basis for the remainder of this work. The a, b, and c geometrical parameters correspond to the inner radius of both ellipses, as seen in Figure 3.3. Wang et al. defined m=a/b and n=a/c as the shape factor of the elliptic rings in the xy plane and the yz plane, respectively [29]. The thickness of each elliptic ring is defined as q_{ab} and q_{bc} for each elliptic ring. The width of the elliptic rings is defined as t_0 and the width of the inner material (colour red in Figure 3.3) is t_1. The relation between these two parameters is defined as T (t_1/t_0). The parameter Φ is the angle between the middle of the inner material and its edge.

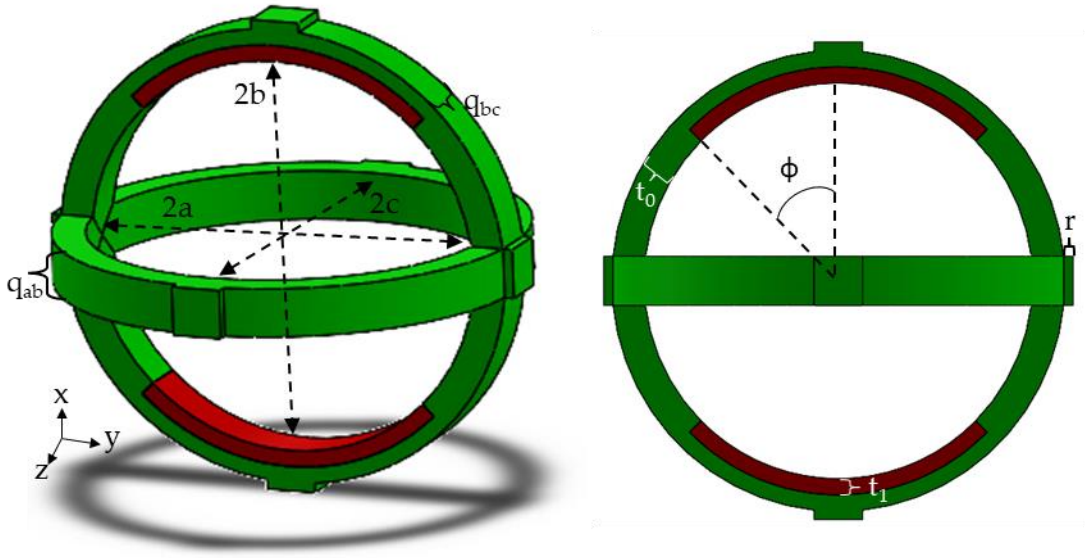

Figure 3.3 - Unit cell parameters.

3.2.3 Study of parameter Φ

The influence of the angle Φ in the anepectic behaviour was studied via FE simulations. The structure used was a 5 x 5 x 5 cell structure with the design parameters shown in Table 3-3.

Table 3-3 - Design parameter of the study of Φ.

a	**m**	**n**	**q_{ab}**	**q_{bc}**	**t_0**	**T**	**r**
(mm)			(mm)	(mm)	(mm)		(mm)
12	1	1	3	3	2	0.5	0.5

The PR and the CTE of the simulated unit cell results are shown in Figure 3.4. The angle Φ varied between 5 º to 75 º with a step of 5 º. To determine the PR a 250 N of load was applied and for the CTE a variation of 200 ºC was used.

As shown in Figure 3.4 a), the parameter Φ doesn't influence the PR obtaining an average value of -0.67 and 0.71 for $\nu_{z,x}$ and $\nu_{z,y}$, respectively. This result was expected since PVA and Nylon have similar stiffnesses.

In Figure 3.4 b), the CLTE α_x tends to achieve more negative values until it reaches a plateau between 35 º and 60 º, stabilizing at an average value of -4.8×10^{-5} ºC. From then on, it increases until the last value studied. It is also relevant to indicate that CLTE value for 5 º is positive, revealing that it doesn't have enough Nylon to reach negative CLTE in the x direction.

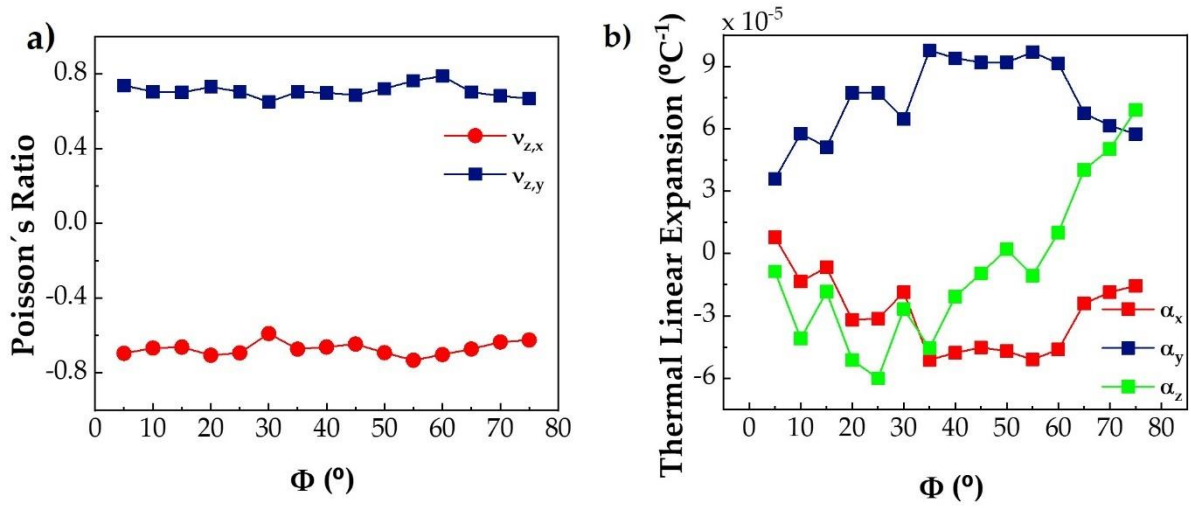

Figure 3.4 - Study of parameter Φ a) PR; b) CTE.

Concerning α_y; it has the same tendency of α_x; with symmetric behaviour, although it only has positive values. This similar tendency shows an inverse relationship between the deformation of the diameter 2b and 2a.

For the third direction, α_z achieved negative values until $\Phi = 45^o$, beyond which it shows increasing values until the end. These results indicate that the CTE of this structure using the parameter Φ is tuneable, making structures with negative CLTE on x direction, z direction, or even on both directions simultaneously possible.

3.3 Manufacturing

To manufacture the structure with PVA and Nylon, optimizing printing parameters and changing some of the initial design parameters (q_{ab}, q_{bc}, and t_0) was necessary. Even after all the changes made, at least one of the rings frequently broke during the printing operation. This phenomenon happens due to the accumulation of material throughout the print in the zone of the overhang. At a particular time, the nozzle hits this accumulation and breaks the ring, even with different printing parameters (printing temperatures, velocities, z hop, and retraction) and design parameters. Appendix E summarizes most of the printing conditions attempted.

The solution found was to separate the structures into parts and assemble them after printing. This way, the printing stage went from 3D to 2D, mitigating all the previous problems caused by the overhang. The structure was broken down into three different basic building parts (design in Appendix F) in order to assemble the final structure (simple example in Figure 3.5). For this assembly, PVA-based white glue (Axton) was used, chosen to limit the influence on the thermomechanical properties of the structures.

Figure 3.5 - Example of an assembly.

Two structures, henceforth called model 1 (Figure 3.6 a) and model 2 (Figure 3.6 b), were manufactured; the difference between them consisting in the incorporation of Nylon in both rings in model 2, while in model 1 only the horizontal rings possessed Nylon inserts. Supports (in blue) were created to ensure the structure was as aligned as possible, while the PVA-based glue solidified. Table 3-4 shows the design parameters used in the two models produced with a 3 x 3 x 3 unit cell.

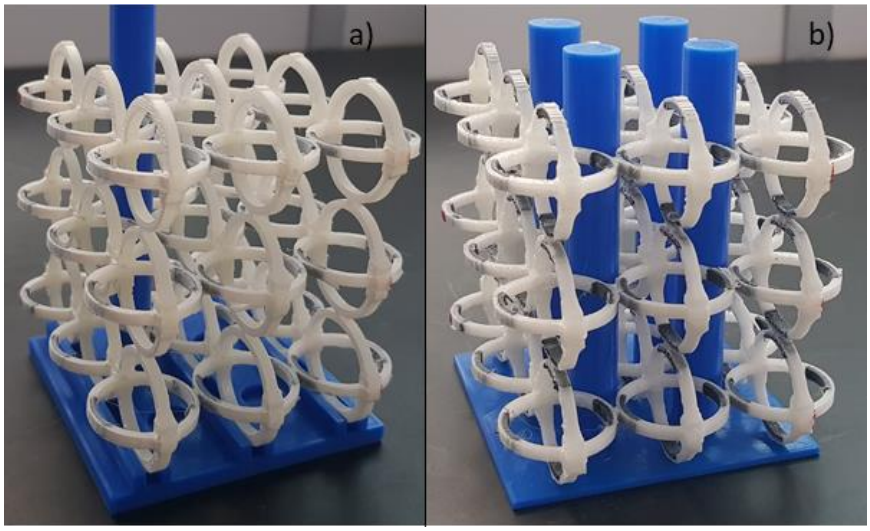

Figure 3.6 - a) Model 1; b) Model 2. PVA is the white material while Nylon is in black.

Table 3-4 - Design parameters of the models.

Parameters	**a**	**m**	**n**	**q_{ab}**	**q_{ac}**	**t_0**	**T**	**r**	**Φ**
Units	mm			mm	mm	mm		mm	º
Model 1	12	1	1	3	3	2	0.5	0.5	30
Model 2	12	1	1	3	3	2	0.5	0.5	30

3.4 Poisson's Ratio

3.4.1 Printed unit cell vs assembled unit cell

A study was carried out to check that the use of PVA-based glue does not significantly affect the mechanical properties of the cell. Integral unit cells (without assembling) were printed with two different printing orientations and submitted to compression. The corresponding stress-strain curves are shown in Appendix G. In Figure 3.7 is possible to observe that fracture occurred between printing layers, irrespective of the printing orientations. This illustrates one of the disadvantages of the FFF technique, the introduction of undesirable anisotropic mechanical properties, in comparison to other techniques. In the sample depicted in Figure 3.7 b) fracture occurred for such a low value of strain that the determination of the PR was impossible.

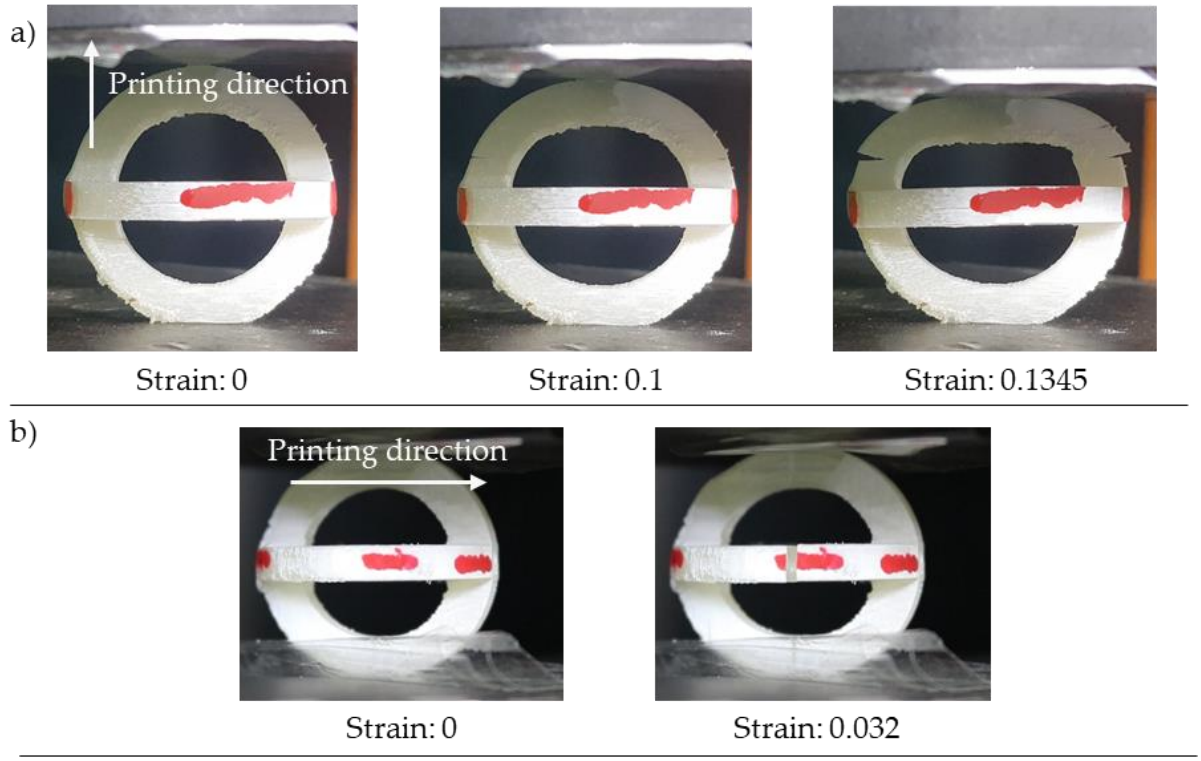

Figure 3.7 - Integral unit cells under compression until fracture.

Figure 3.8 presents an assembled unit cell that achieved the predicted PR value, denoting a partially auxetic behaviour. Because of the printing orientation of the assembled pieces, the unit cell supports compression better than the none assembled unit cells. Concluding that due to the printing orientation, printing in separate pieces allows the observation of deformation up to higher levels of strain (Appendix G).

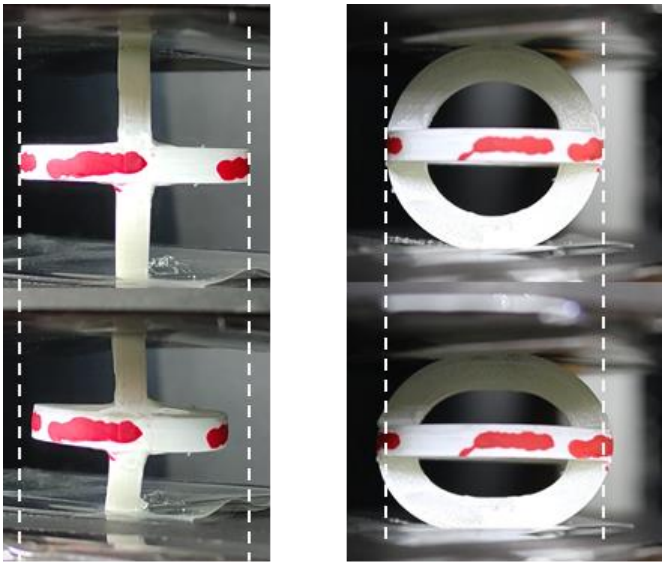

Figure 3.8 - Assembled unit cell under compression.

Nevertheless, some of the assembled samples failed at the junction zone in the beginning of the tests, as seen in Figure 3.9. This was probably due to the low amount of PVA glue, that did not allow a good joint between the assembled parts. So, it is possible to conclude that to obtain a properly assembled cell, it is necessary to ensure proper coverage of the junctions by the glue, so as to obtain the best adhesion possible.

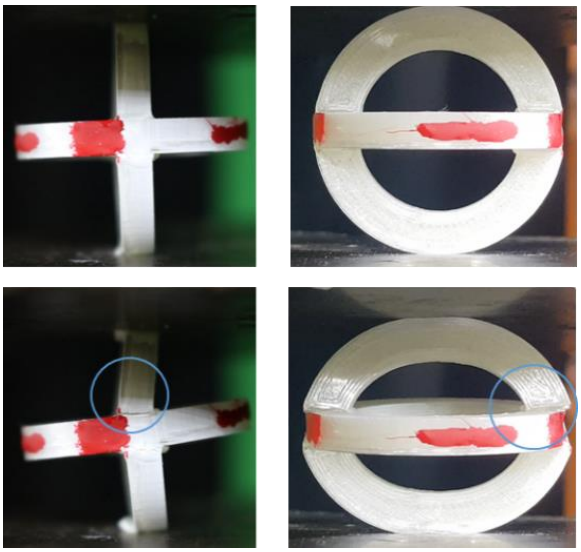

Figure 3.9 - Compressive test of an assembly cell unit with low amount of glue.

Figure 3.10 shows the average PR of the assembled cells. The explanation of the PR calculation and the PR curves of all the samples is displayed in Appendix H. The $\nu_{z,y}$ exhibit positive values while $\nu_{z,x}$ had values below zero. This was expected as this behaviour was observed previously in the FE analysis. Beyond that, similar results were obtained in the investigation conducted by Wang et al [29].

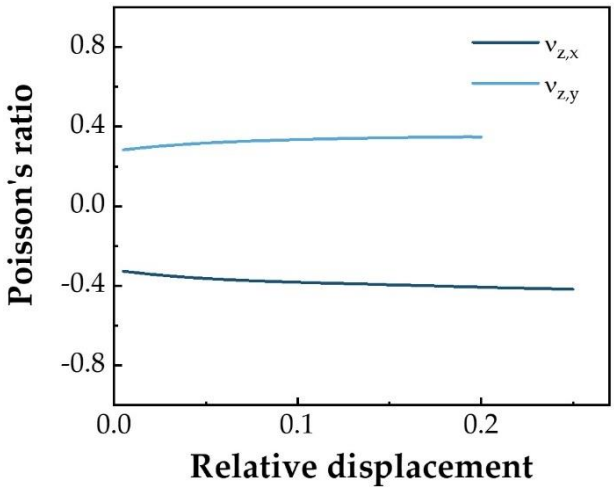

Figure 3.10 - Average PR of the assembled cells.

3.4.2 2 x 2 x 2 structure

Structures formed by 2 x 2 x 2 unit cells, based on model 1 were manufactured, in order to check if an assembled structure does not fracture in the junction zone under low strain. The corresponding stress-strain curves are shown in Appendix I.

Figure 3.11 shows the average values of the $\nu_{z,x}$ and $\nu_{z,y}$. It is possible to conclude that the structure has a partially auxetic behaviour, as expected. Individually measured PR values, accompanied by an explanation of the PR calculation method are provided in Appendix J. Outliers, probably caused by the camera's resolution, were not considered for average calculation.

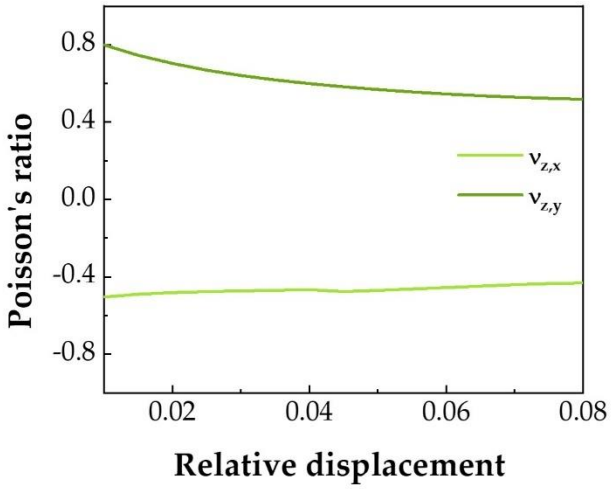

Figure 3.11 - PR of a 2 x 2 x 2 structure of model 1.

3.4.3 3 x 3 x 3 structure

Structures based on both models 1 and 2 were assembled as 3 × 3 × 3 arrays and tested under compression to confirm their auxetic behaviour on the xz plane and a positive PR on the yz plane (Appendix K). The average results are shown in Figure 3.12. Appendix L explains the PR calculation of these structures and presents all the samples PR curves. Some samples have unusual values between 0.01 and 0.025 of strain, most likely because of the camera's resolution (the higher the resolution, the larger the number of pixels, hence the more precise the data).

Figure 3.12 a) and b) describe the PR of the structure throughout the relative displacement range tested. As expected from the simulation predictions, the $\nu_{z,x}$ and $\nu_{z,y}$ obtained positive and negative values, respectively. The PR of the central cell (Figure 3.12 c) and d)) demonstrate a similar behaviour to the overall structure's PR.

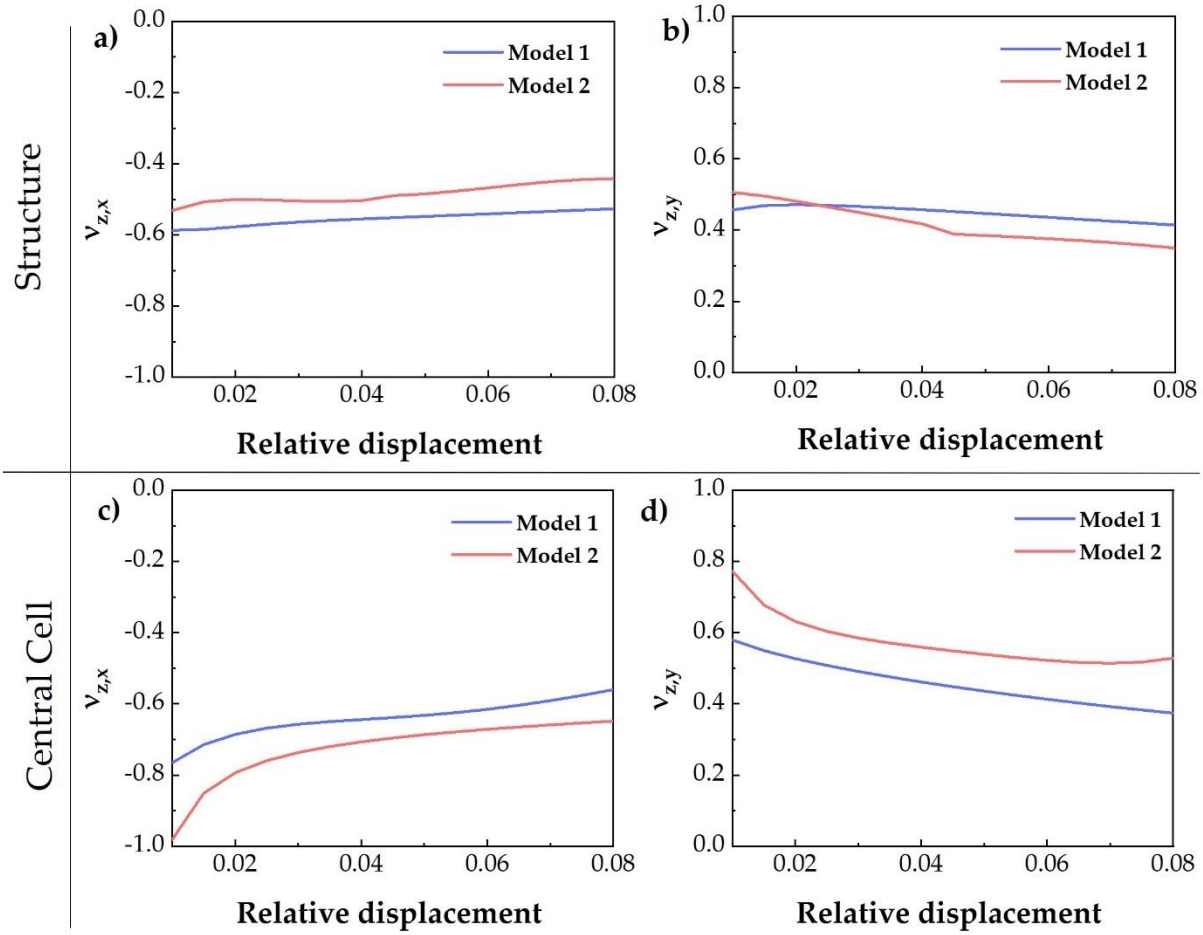

Figure 3.12 - Poisson's Ratio of model 1 and 2 throughout the experiment.

It is also possible to conclude that models 1 and 2 do not exhibit similar PR values. This could be because of the different amounts of Nylon, effecting the stiffness of the structure, and thus influencing the PR.

Beyond that, throughout the mechanical test, the PR in both directions is not constant, decreasing in absolute value; probably due to the progressive change in the shape of the rings (Figure 3.13). Alternatively, the observed effect could be due to edge effect and parallax errors.

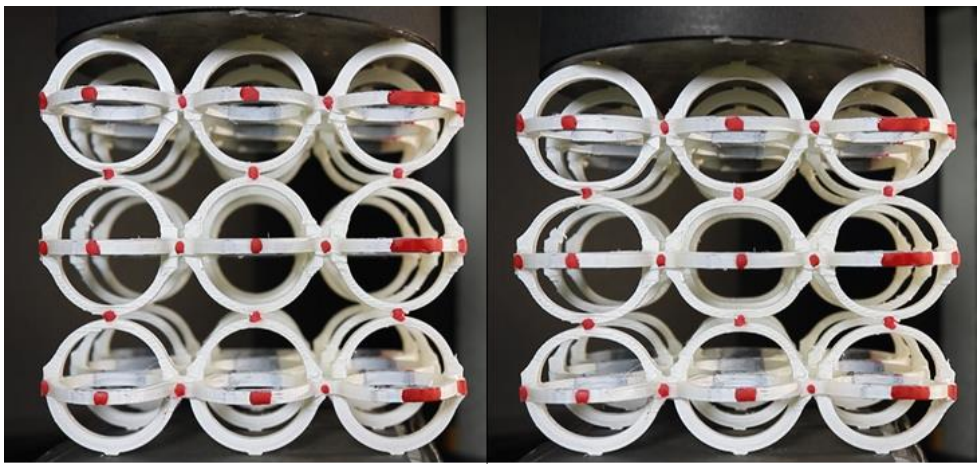

Figure 3.13 - Example of the view yz of a structure (model 1) deformed.

3.4.4 Influence of the number of cells

In order to identify how the PR is influenced by the number of cells, a comparison of unit cell, 2 x 2 x 2 and 3 x 3 x 3 structures was performed. Figure 3.14 shows this study.

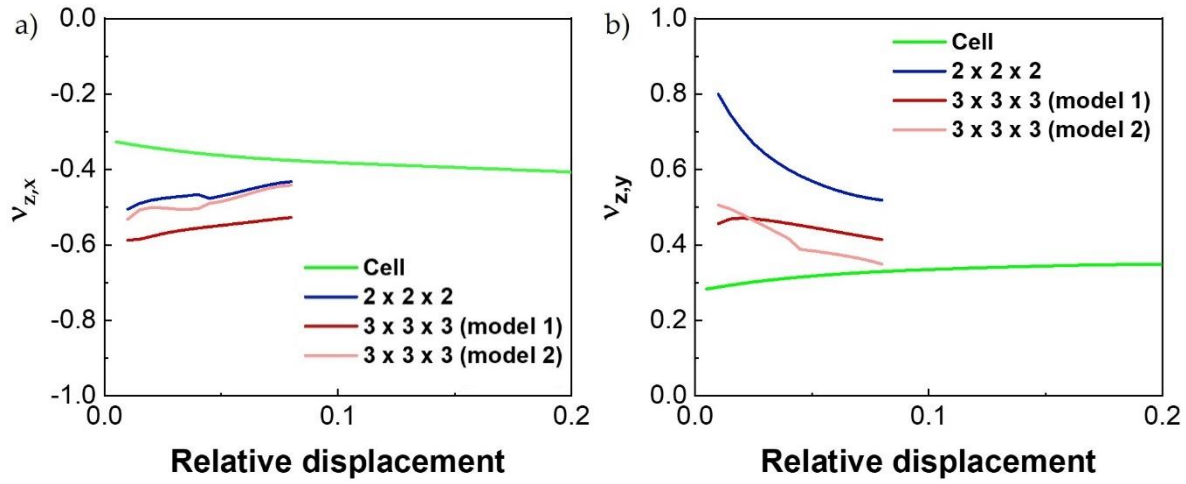

Figure 3.14-Influence of the number of cells in PR.

With the exception of the $\nu_{z,y}$ values of the 2 x 2 x 2 structure, it is possible to observe the existence of a strong correlation between the number of cells and the values of PR. As the number of cells increases, the $\nu_{z,x}$ becomes more negative, while $\nu_{z,y}$ turns more positive.

3.5 Coefficient of thermal expansion

To determine the CLTE, thermal tests were carried out on models 1 and 2. Beyond that, a single material structure was manufactured from PVA and tested as a control sample. Due to this methodology, it was possible to determine value of α_z in two different planes. The explanation of the CLTE calculation for the 3 x 3 x 3 structure is presented in Appendix M. The thermal experiment was tested from room temperature (around 21 ° C) up to 80 ° C.

Using three thermocouples in different positions near the sample, it was possible to observe a variation in the glycerol temperature throughout the experiment. In all the performed experiments, the largest difference between the temperature of the thermocouples was below 5 °C. Due to this error, it was decided to calculate the CLTE every 10 °C, giving a variation of ± 2.5 °C. Figure 3.15 show an example of one of the experiments, where the average of the thermocouples is presented in green and the red band corresponds to the ± 2.5 °C margin around the average. Observation of the graph lead to the conclusion that none of the channels surpasses this variation.

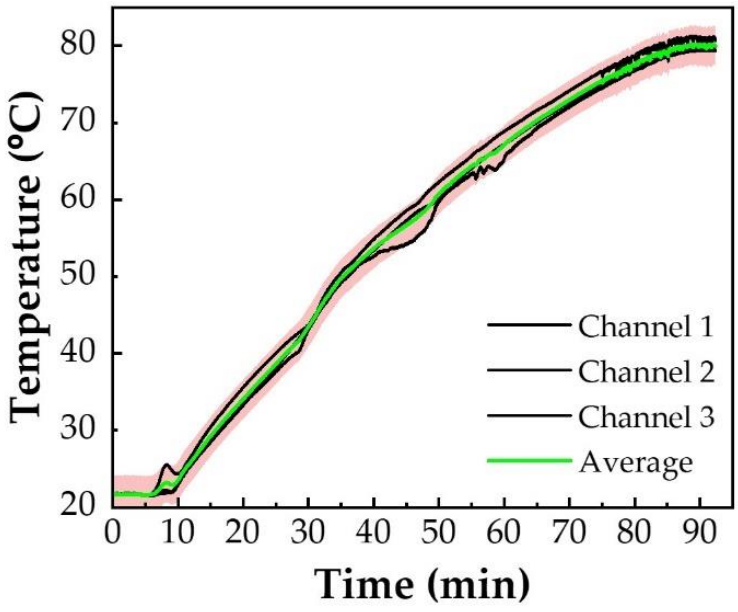

Figure 3.15 - Temperature registered of three thermocouples and their average throughout a thermal experiment. The red area represents the ± 2.5 °C variation of the average.

3.5.1 Study of model 1

Figure 3.16 shows the CLTE expansion in the three directions, x, y, and z, of model 1. In all directions, the CLTE was positive throughout the experiment. This result was unexpected, since the FE simulation of a similar structure offers negative values for both α_x and α_z.

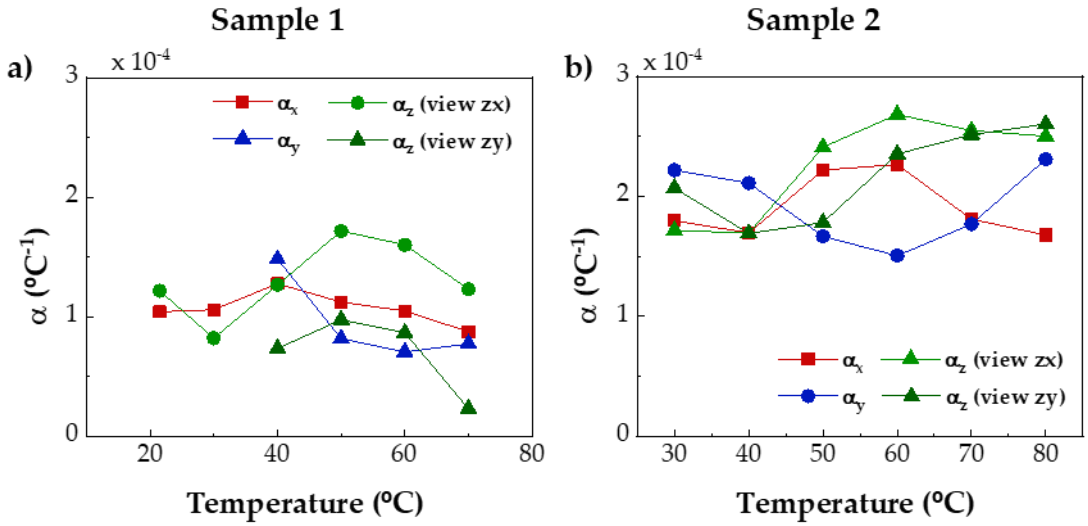

Figure 3.16 - CLTE of model 1 a) sample 1; b) sample 2.

3.5.2 Study of model 2

The CLTE of model 2 was determined along the x, y, and z directions, as shown in Figure 3.17. The structure has a negative thermal expansion in two different directions, x, and z. This result was expected, as the expansion of nylon creates a deformation similar to that resulting from a compressive stress, resulting in α_x and α_z being negative and α_y positive.

It is also observed that both α_x and α_z achieved positive values at 30 ºC. After that, the values of the two CLTE decreased until the end of the experiment. This occurrence is, most likely, due to the structure only being capable of anepectic behaviour above the constituent materials' T_g, as already observed for 2D anepectic meshes by Raminhos et al. [58].

Due to the methodology used, it is possible to determine α_z in two different views throughout the test. According to Figure 3.17, this parameter presents similar behaviour and values in both views, demonstrating that the results and the method created are reliable, slight variations notwithstanding.

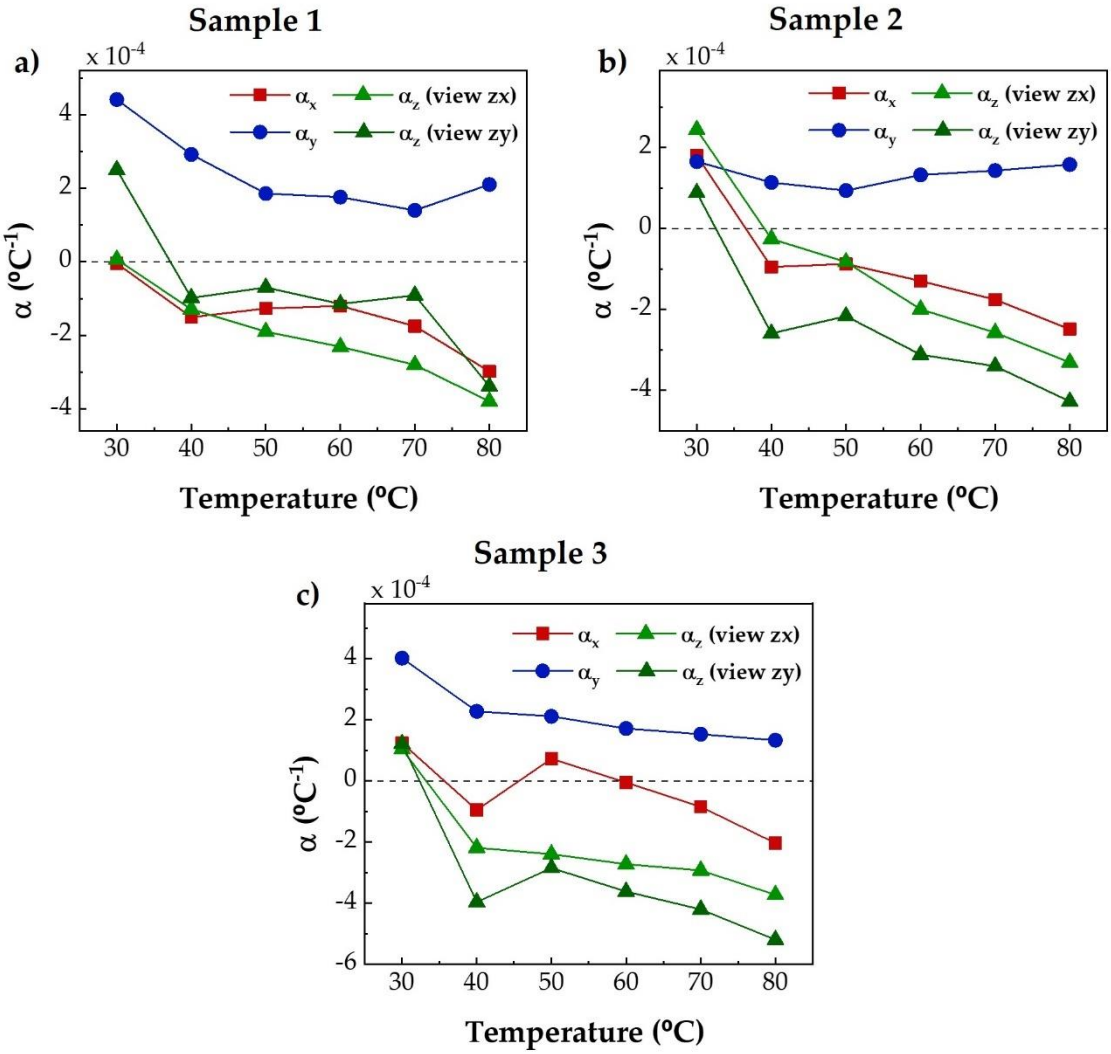

Figure 3.17 - CLTE of model 2 a) sample 1; b) sample 2; c) sample 3.

After these results, it is possible to conclude that the manufactured model 2 exhibited the intended anepectic behaviour.

3.5.3 Single material DER structure

The results of the thermal test of the single material DER structure, manufactured from PVA, are shown in Figure 3.18. It is possible to conclude that this structure, which is constituted of one material with positive CTE, obtained a negative CTE. This result is unexpected because it was not found in the literature a NTE metamaterial composed of one positive CTE material. It is relevant to point out that according to the literature, it was observed the opposite. Until now, a NTE metamaterial was achieved only when constituted of two materials, but the same metamaterial had a positive CTE when composed by one material [58], [78], [79].

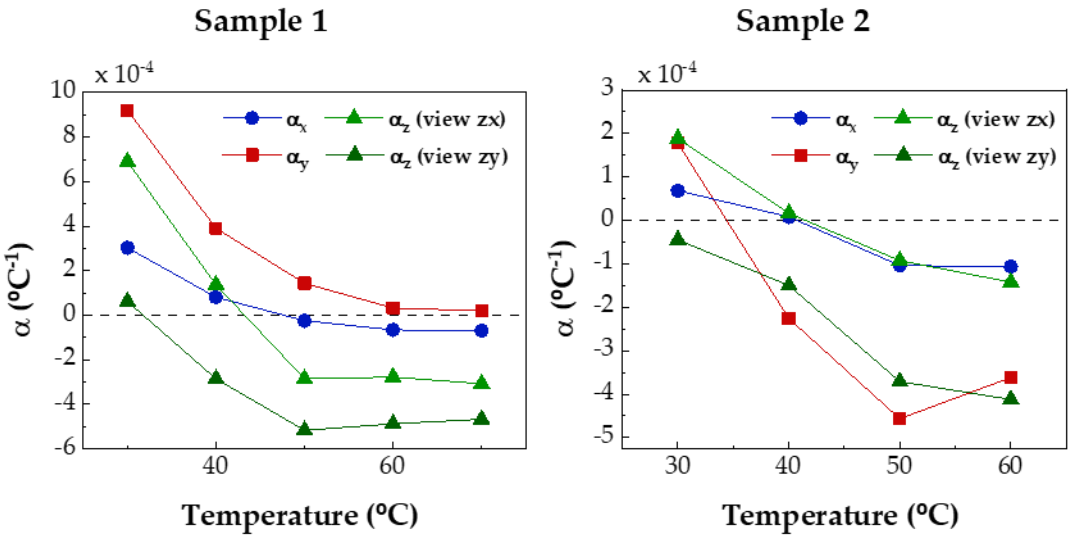

Figure 3.18 - CLTE of 3 x 3 x 3 DER structure of PVA a) sample 1; b) sample 2.

This NTE of a single material structure may be occurring due to the intrinsic geometry anisotropy. Despite that, as it is the first single material structure with this behaviour it is necessary to perform more tests to confirm these results.

4

CONCLUSIONS AND FUTURE PERSPECTIVES

So far, the anepectic behaviour of 3D structures had only been demonstrated numerically by finite element (FE) or analytical analysis. Therefore, the breakthrough achieved with current work consisted in manufacturing and experimentally validating the anepectic behaviour of a 3D structure.

The influence of the printing orientation on the mechanical results were investigated. It was possible to conclude that it has a massive impact on the final properties of 3D printed material.

FE analysis was performed to obtain a 3D anepectic unit cell, in other words, with a negative Poisson's Ratio (PR) and a negative coefficient of thermal expansion (CTE). In order to achieve these properties, the incorporation of a second material in the unit cell developed by Wang et al. [29] was required. The chosen materials were PVA and Nylon due to the similar stiffness values but different CTE. All the design parameters of the unit cell studied were then defined.

Two 3D models were designed based on the unit cell developed. The difference between them is the amount of Nylon in each unit cell of the 3 x 3 x 3 structure. Both models were manufactured through a FFF technique, and Poisson's ratio and coefficient of thermal expansion were characterized. Model 2 (with Nylon in both rings) obtained an anepectic behaviour. A negative value was observed for $\nu_{z,x}$, while $\nu_{z,y}$ was positive throughout the compressive test. The linear coefficient of thermal expansion in the x and z direction was negative, whereas the value was positive in the y direction.

A study of the influence of the number of cells on the PR values was made. As the number of cells increases, the PR tends to increase in module. However, it is relevant to deepen

this study since it was carried out only from the unit cell to the 3 x 3 x 3 structure due to the higher printing time. A similar study for CTE would be interesting to perform.

As a future perspective, it is relevant to study the influence of all the design parameters stated previously in this work. This parametric study allows to understand each parameter's influence and thus choose the appropriate parametric values for the application. The use of FE simulation will be a reliable tool to understand the behaviour of each parameter. As noted in chapter 3.2.3, a parameter change may have a high impact on the thermal and mechanical properties of the structure, being possible to change from negative to positive values. Beyond that, as a future perspective, the manufacture of the unit cell of Figure D.1 c) and characterization of the anepectic behaviour could be another way of transforming a DER structure into an anepectic metamaterial.

It might be relevant the study of different geometries beyond ellipses. A simulation study by FE method was made on a hexagonal and octagonal unit cell (Figure 4.1 a) and b)), both presented a NTE behaviour. This preview result not only shows the possibility of manufacturing an anepectic metamaterial similar to the DER structure with different geometry, as is another parameter to tailor the anepectic behaviour of these types of structures. Printing these geometries with a FFF printer is less challenging due to a less accumulation of material on the overhang as the printing angle of the overhang is higher. An example of a 2 x 2 x 2 structure with a hexagonal geometry printed is shown in Appendix N.

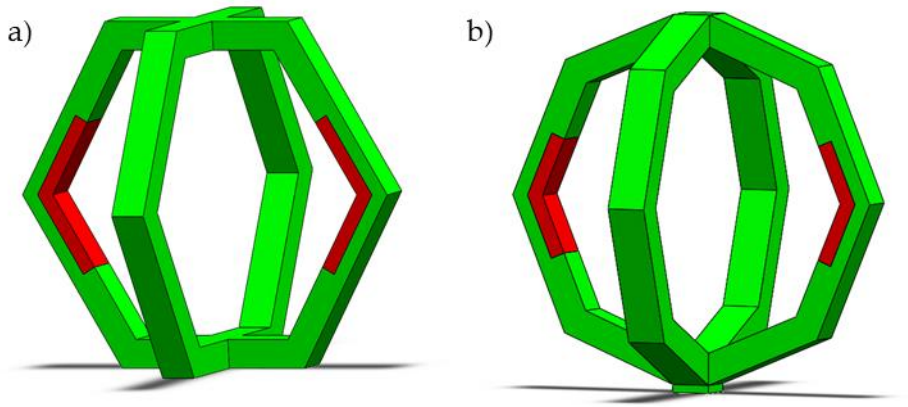

Figure 4.1 - Unit cell with different geometry. a) hexagonal unit cell; b) octagonal unit cell.

One of the difficulties of this work was the creation of a new methodology that would allow the determination of the linear thermal expansion coefficient for a 3D anepectic structure in the three directions. Since it was difficult to get the sample immobilized in a container with moving glycerol to obtain a homogeneous temperature and not restrict all its movement, as it will influence the thermal expansion of the structure. Thus, it would be necessary to optimize this methodology or create a better one.

Furthermore, Wang et al., based on a structure similar to DER, manufactured a structure in which the cells undergo a 90 º rotation along the x and y axis (Figure 4.2) to obtain an auxetic behaviour in both directions [29]. Due to this behaviour, it would be interesting to replace part of the structure with a second material to obtain an anepectic behaviour, as performed in the present work. Then investigate if it would obtain negative values in all directions, both in PR and LCTE.

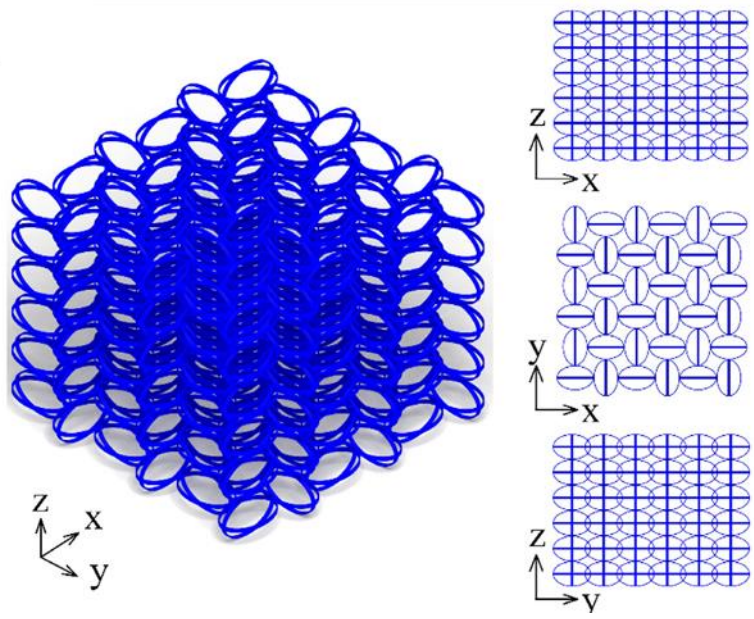

Figure 4.2 - Structure developed by Wang et al.[29]

From a future perspective, it would be interesting to realise thermal cycles during the thermal tests to observe if the anepectic behaviour changes throughout the cycles. Furthermore, it would be interesting to submerge the structures into a high temperature glycerol container to determine the reaction time.

Thermal tests were carried on a 3 x 3 x 3 structure of one material (PVA) and obtained a NTE. This result was unexpected since it is the first time that a metamaterial composed of one material with positive CTE obtained a NTE. For that reason, it is essential to reproduce these results to confirm it.

REFERENCES

[1] X. Ren, R. Das, P. Tran, T. D. Ngo, and Y. M. Xie, "Auxetic metamaterials and structures: A review," *Smart Materials and Structures*, vol. 27, no. 2. p. 023001, 24-Jan-2018, doi: 10.1088/1361-665X/aaa61c.

[2] T.-C. Lim, "Introduction," in *Mechanics of Metamaterials with Negative Parameters*, Singapore: Springer, Singapore, 2020, pp. 1–8.

[3] L. Ai and X. L. Gao, "Metamaterials with negative Poisson's ratio and non-positive thermal expansion," *Compos. Struct.*, vol. 162, pp. 70–84, Feb. 2017, doi: 10.1016/j.compstruct.2016.11.056.

[4] X.-L. Peng and S. Bargmann, "A novel hybrid-honeycomb structure: Enhanced stiffness, tunable auxeticity and negative thermal expansion," *Int. J. Mech. Sci.*, vol. 190, p. 106021, 2021, doi: https://doi.org/10.1016/j.ijmecsci.2020.106021.

[5] J. O. Cardoso, J. P. Borges, and A. Velhinho, "Structural metamaterials with negative mechanical/thermomechanical indices: A review," *Prog. Nat. Sci. Mater. Int.*, Nov. 2021, doi: 10.1016/J.PNSC.2021.10.015.

[6] J. C. Bose, "On the rotation of plane of polarisation of electric wave by a twisted structure," *Proc. R. Soc. London*, vol. 63, no. 389–400, pp. 146–152, Dec. 1898, doi: 10.1098/rspl.1898.0019.

[7] X. Yu, J. Zhou, H. Liang, Z. Jiang, and L. Wu, "Mechanical metamaterials associated with stiffness, rigidity and compressibility: A brief review," *Progress in Materials Science*, vol. 94. pp. 114–173, 01-May-2018, doi: 10.1016/j.pmatsci.2017.12.003.

[8] J. U. Surjadi *et al.*, "Mechanical Metamaterials and Their Engineering Applications," *Adv. Eng. Mater.*, vol. 21, no. 3, p. 1800864, Mar. 2019, doi: 10.1002/adem.201800864.

[9] K. Wei, Y. Peng, Z. Qu, Y. Pei, and D. Fang, "A cellular metastructure incorporating coupled negative thermal expansion and negative Poisson's ratio," *Int. J. Solids Struct.*, vol. 150, pp. 255–267, Oct. 2018, doi: 10.1016/j.ijsolstr.2018.06.018.

[10] T. Li, Y. Chen, X. Hu, Y. Li, and L. Wang, "Exploiting negative Poisson's ratio to design 3D-printed composites with enhanced mechanical properties," *Mater. Des.*, vol. 142, pp. 247–258, Mar. 2018, doi: 10.1016/j.matdes.2018.01.034.

[11] T.-C. Lim, "Auxetic and Negative Thermal Expansion Structure Based on Interconnected Array of Rings and Sliding Rods," *Phys. status solidi*, vol. 254, no. 12, p. 1600775, Dec. 2017, doi: 10.1002/pssb.201600775.

[12] J. N. Grima *et al.*, "Natrolite: A zeolite with negative Poisson's ratios," *J. Appl. Phys.*, vol. 101, no. 8, p. 086102, Apr. 2007, doi: 10.1063/1.2718879.

[13] M. Siddorn, F. X. Coudert, K. E. Evans, and A. Marmier, "A systematic typology for negative Poisson's ratio materials and the prediction of complete auxeticity in pure silica zeolite JST," *Phys. Chem. Chem. Phys.*, vol. 17, no. 27, pp. 17927–17933, Jul. 2015, doi: 10.1039/c5cp01168j.

[14] Z. Qin, G. Qin, and M. Hu, "Origin of anisotropic negative Poisson's ratio in graphene," *Nanoscale*, vol. 10, no. 22, pp. 10365–10370, Jun. 2018, doi: 10.1039/c8nr00696b.

[15] J. W. Jiang and H. S. Park, "Negative Poisson's Ratio in Single-Layer Graphene Ribbons," *Nano Lett.*, vol. 16, no. 4, pp. 2657–2662, Apr. 2016, doi: 10.1021/acs.nanolett.6b00311.

[16] A. Yeganeh-Haeri, D. J. Weidner, and J. B. Parise, "Elasticity of α-cristobalite: A silicon dioxide with a negative poisson's ratio," *Science (80-.).*, vol. 257, no. 5070, pp. 650–652, Jul. 1992, doi: 10.1126/science.257.5070.650.

[17] Z. Gao, X. Dong, N. Li, and J. Ren, "Novel Two-Dimensional Silicon Dioxide with in-Plane Negative Poisson's Ratio," *Nano Lett.*, vol. 17, no. 2, pp. 772–777, Feb. 2017, doi: 10.1021/acs.nanolett.6b03921.

[18] D. Li, R. Gao, L. Dong, W. K. Lam, and F. Zhang, "A novel 3D re-entrant unit cell structure with negative Poisson's ratio and tunable stiffness," *Smart Mater. Struct.*, vol. 29, no. 4, p. 045015, Mar. 2020, doi: 10.1088/1361-665X/ab6696.

[19] J. Xiong, D. Gu, H. Chen, D. Dai, and Q. Shi, "Structural optimization of re-entrant negative Poisson's ratio structure fabricated by selective laser melting," *Mater. Des.*, vol. 120, pp. 307–316, Apr. 2017, doi: 10.1016/j.matdes.2017.02.022.

[20] C. Li, H. S. Shen, and H. Wang, "Nonlinear bending of sandwich beams with functionally graded negative Poisson's ratio honeycomb core," *Compos. Struct.*, vol. 212, pp. 317–325, Mar. 2019, doi: 10.1016/j.compstruct.2019.01.020.

[21] J. Qiao and C. Q. Chen, "Analyses on the in-plane impact resistance of auxetic double arrowhead honeycombs," *J. Appl. Mech. Trans. ASME*, vol. 82, no. 5, pp. 051007–051006, May 2015, doi: 10.1115/1.4030007.

[22] T.-C. Lim, "A 3D auxetic material based on intersecting double arrowheads," *Phys. status solidi*, vol. 253, no. 7, pp. 1252–1260, Jul. 2016, doi: 10.1002/pssb.201600015.

[23] L. Gu, Q. Xu, D. Zheng, H. Zou, Z. Liu, and Z. Du, "Analysis of the mechanical properties of double arrowhead auxetic metamaterials under tension," *Text. Res. J.*, vol. 90, no. 21–22, pp. 2411–2427, Nov. 2020, doi: 10.1177/0040517520924850.

[24] L. Mizzi *et al.*, "Mechanical metamaterials with star-shaped pores exhibiting negative and zero Poisson's ratio," *Mater. Des.*, vol. 146, pp. 28–37, May 2018, doi: 10.1016/j.matdes.2018.02.051.

[25] M. S. Rad, Z. Ahmad, and A. Alias, "Computational approach in formulating mechanical characteristics of 3D star honeycomb auxetic structure," *Adv. Mater. Sci. Eng.*, vol. 2015, 2015, doi: 10.1155/2015/650769.

[26] D. Attard and J. N. Grima, "Auxetic behaviour from rotating rhombi," *Phys. status solidi*, vol. 245, no. 11, pp. 2395–2404, Nov. 2008, doi: 10.1002/pssb.200880269.

[27] D. Attard, E. Manicaro, and J. N. Grima, "On rotating rigid parallelograms and their potential for exhibiting auxetic behaviour," *Phys. status solidi*, vol. 246, no. 9, pp. 2033–2044, Sep. 2009, doi: 10.1002/pssb.200982034.

[28] K. K. Dudek *et al.*, "On the dynamics and control of mechanical properties of hierarchical rotating rigid unit auxetics," *Sci. Rep.*, vol. 7, no. 1, pp. 1–9, Apr. 2017, doi: 10.1038/srep46529.

[29] L. Wang *et al.*, "Latitude-and-longitude-inspired three-dimensional auxetic metamaterials," *Extrem. Mech. Lett.*, vol. 42, p. 101142, Jan. 2021, doi: 10.1016/j.eml.2020.101142.

[30] T.-C. Lim, "Negative Environmental Expansion for Interconnected Array of Rings and Sliding Rods," *Phys. status solidi*, vol. 256, no. 1, p. 1800032, Jan. 2019, doi: 10.1002/pssb.201800032.

[31] W. Wu, X. Song, J. Liang, R. Xia, G. Qian, and D. Fang, "Mechanical properties of anti-tetrachiral auxetic stents," *Compos. Struct.*, vol. 185, pp. 381–392, Feb. 2018, doi: 10.1016/j.compstruct.2017.11.048.

[32] M. N. Ali and I. U. Rehman, "An Auxetic structure configured as oesophageal stent with potential to be used for palliative treatment of oesophageal cancer; Development and in vitro mechanical analysis," *J. Mater. Sci. Mater. Med.*, vol. 22, no. 11, pp. 2573–2581, Nov. 2011, doi: 10.1007/s10856-011-4436-y.

[33] C. Anurag, C. Kesava Anvesh, and A. S. Harsha, "Auxetic Materials," *Int. J. TRENDS Eng. Technol.*, vol. 5, no. 2, pp. 156–160, 2015.

[34] A. Alderson and K. Alderson, "Expanding materials and applications: Exploiting auxetic textiles," *Tech. Text. Int.*, vol. 14, no. 6, pp. 29–34, 2005.

[35] Z. Wang and H. Hu, "Auxetic materials and their potential applications in textiles," *Text. Res. J.*, vol. 84, no. 15, pp. 1600–1611, Sep. 2014, doi: 10.1177/0040517512449051.

[36] W. Miller, C. W. Smith, D. S. MacKenzie, and K. E. Evans, "Negative thermal expansion: A review," *Journal of Materials Science*, vol. 44, no. 20. Springer, pp. 5441–5451, 02-Oct-2009, doi: 10.1007/s10853-009-3692-4.

[37] K. Takenaka, "Progress of research in negative thermal expansion materials: Paradigm shift in the control of thermal expansion," *Frontiers in Chemistry*, vol. 6, no. JUL. p. 267, 02-Jul-2018, doi: 10.3389/fchem.2018.00267.

[38] G. D. Barrera, J. A. O. Bruno, T. H. K. Barron, and N. L. Allan, "Negative thermal expansion," *Journal of Physics Condensed Matter*, vol. 17, no. 4. p. R217, 02-Feb-2005, doi: 10.1088/0953-8984/17/4/R03.

[39] Q. Wang, J. A. Jackson, Q. Ge, J. B. Hopkins, C. M. Spadaccini, and N. X. Fang, "Lightweight Mechanical Metamaterials with Tunable Negative Thermal Expansion," *Phys. Rev. Lett.*, vol. 117, no. 17, p. 175901, Oct. 2016, doi: 10.1103/PhysRevLett.117.175901.

[40] N. Shi *et al.*, "Strong Negative Thermal Expansion of Cu 2 PVO 7 in a Wide Temperature Range," *Chem. Mater.*, vol. 33, no. 4, pp. 1321–1329, Feb. 2021, doi: 10.1021/acs.chemmater.0c04336.

[41] B. A. Marinkovic, P. M. Jardim, R. R. De Avillez, and F. Rizzo, "Negative thermal expansion in Y2Mo3O12," *Solid State Sci.*, vol. 7, no. 11, pp. 1377–1383, Nov. 2005, doi:

10.1016/j.solidstatesciences.2005.08.012.

[42] P. M. Forster, A. Yokochi, and A. W. Sleight, "Enhanced Negative Thermal Expansion in Lu 2 W 3 O 12," *Journal of Solid State Chemistry*, vol. 140, no. 1. pp. 157–158, 01-Oct-1998, doi: 10.1006/jssc.1998.7967.

[43] M. Ducamp and F.-X. Coudert, "Systematic Study of the Thermal Properties of Zeolitic Frameworks," *ChemRxiv*, Jan. 2021, doi: 10.26434/CHEMRXIV.13606763.V1.

[44] D. A. Woodcock, P. Lightfoot, P. A. Wright, L. A. Villaescusa, M. J. Díaz-Cabañas, and M. A. Camblor, "Strong negative thermal expansion in the siliceous zeolites ITQ-1, ITQ-3 and SSZ-23," *J. Mater. Chem.*, vol. 9, no. 2, pp. 349–351, Jan. 1999, doi: 10.1039/a808059c.

[45] C. L. Choy, F. C. Chen, and K. Young, "Negative thermal expansion in oriented crystalline polymers," *J. Polym. Sci. Polym. Phys. Ed.*, vol. 19, no. 2, pp. 335–352, Feb. 1981, doi: 10.1002/pol.1981.180190213.

[46] R. H. Baughman and E. A. Turi, "Negative thermal expansion of a polydiacetylene single crystal," *J. Polym. Sci. Part A-2 Polym. Phys.*, vol. 11, no. 12, pp. 2453–2466, Dec. 1973, doi: 10.1002/pol.1973.180111213.

[47] K. Takenaka, "Negative thermal expansion materials: Technological key for control of thermal expansion," *Science and Technology of Advanced Materials*, vol. 13, no. 1. p. 11, 02-Feb-2012, doi: 10.1088/1468-6996/13/1/013001.

[48] J. N. Grima, V. Zammit, and R. Gatt, "Negative Thermal Expansion," Malta Chamber of Scientists, 2006.

[49] K. Wei, X. Xiao, W. Xu, Z. Han, Y. Wu, and Z. Wang, "Large programmable coefficient of thermal expansion in additively manufactured bi-material mechanical metamaterial," *Virtual Phys. Prototyp.*, vol. 16, no. S1, pp. S53–S65, 2021, doi: 10.1080/17452759.2021.1917295.

[50] J. Li, Q. Yang, Y. Wei, N. Huang, and R. Tao, "A synergistic design of composite metamaterial with drastically tailorable thermal expansion and Poisson's ratio," *Compos. Struct.*, vol. 275, p. 114446, Nov. 2021, doi: 10.1016/J.COMPSTRUCT.2021.114446.

[51] E. M. Parsons, "Lightweight cellular metal composites with zero and tunable thermal expansion enabled by ultrasonic additive manufacturing: Modeling, manufacturing, and testing," *Compos. Struct.*, vol. 223, p. 110656, Sep. 2019, doi: 10.1016/J.COMPSTRUCT.2019.02.031.

[52] X. Li, L. Gao, W. Zhou, Y. Wang, and Y. Lu, "Novel 2D metamaterials with negative Poisson's ratio and negative thermal expansion," *Extrem. Mech. Lett.*, vol. 30, p. 100498, Jul. 2019, doi: 10.1016/j.eml.2019.100498.

[53] M. Fu, J. Huang, B. Zheng, Y. Chen, and C. Huang, "Three-dimensional auxetic materials with controllable thermal expansion," *Smart Mater. Struct.*, vol. 29, no. 8, p. 085034, Aug. 2020, doi: 10.1088/1361-665X/ab9dda.

[54] L. Wu, B. Li, and J. Zhou, "Isotropic Negative Thermal Expansion Metamaterials," *ACS Appl. Mater. Interfaces*, vol. 8, no. 27, pp. 17721–17727, Jul. 2016, doi: 10.1021/acsami.6b05717.

[55] K. Wei, Y. Peng, K. Wang, S. Duan, X. Yang, and W. Wen, "Three dimensional

lightweight lattice structures with large positive, zero and negative thermal expansion," *Compos. Struct.*, vol. 188, pp. 287–296, Mar. 2018, doi: 10.1016/j.compstruct.2018.01.030.

[56] A. W. Sleight, "Negative thermal expansion materials," *Curr. Opin. Solid State Mater. Sci.*, vol. 3, no. 2, pp. 128–131, Apr. 1998, doi: 10.1016/S1359-0286(98)80076-4.

[57] T.-C. Lim, "Negative thermal expansion in transversely isotropic space frame trusses," *Phys. status solidi*, vol. 250, no. 10, pp. 2062–2069, Oct. 2013, doi: 10.1002/pssb.201384234.

[58] J. S. Raminhos, J. P. Borges, and A. Velhinho, "Development of polymeric anepectic meshes: auxetic metamaterials with negative thermal expansion," *Smart Mater. Struct.*, vol. 28, no. 4, p. 45010, 2019, doi: 10.1088/1361-665x/ab034b.

[59] J. N. Grima, P. S. Farrugia, R. Gatt, and V. Zammit, "Connected triangles exhibiting negative Poisson's ratios and negative thermal expansion," *J. Phys. Soc. Japan*, vol. 76, no. 2, Feb. 2007, doi: 10.1143/JPSJ.76.025001.

[60] C. K. Ng, K. K. Saxena, R. Das, and E. I. Saavedra Flores, "On the anisotropic and negative thermal expansion from dual-material re-entrant-type cellular metamaterials," *J. Mater. Sci.*, vol. 52, no. 2, pp. 899–912, Jan. 2017, doi: 10.1007/s10853-016-0385-7.

[61] T. C. Lim, "A class of shape-shifting composite metamaterial honeycomb structures with thermally-adaptive Poisson's ratio signs," *Compos. Struct.*, vol. 226, p. 111256, Oct. 2019, doi: 10.1016/J.COMPSTRUCT.2019.111256.

[62] C. S. Ha, E. Hestekin, J. Li, M. E. Plesha, and R. S. Lakes, "Controllable thermal expansion of large magnitude in chiral negative Poisson's ratio lattices," *Phys. status solidi*, vol. 252, no. 7, pp. 1431–1434, Jul. 2015, doi: 10.1002/pssb.201552158.

[63] L. Ai and X. L. Gao, "Three-dimensional metamaterials with a negative Poisson's ratio and a non-positive coefficient of thermal expansion," *Int. J. Mech. Sci.*, vol. 135, pp. 101–113, Jan. 2018, doi: 10.1016/j.ijmecsci.2017.10.042.

[64] M. M. Chen, M. H. Fu, L. H. Lan, and S. V. Sheshenin, "A novel 3D structure with tunable Poisson's ratio and tailorable coefficient of thermal expansion based on a tri-material triangle unit," *Compos. Struct.*, vol. 253, p. 112803, Dec. 2020, doi: 10.1016/j.compstruct.2020.112803.

[65] N. Xu and H. T. Liu, "A novel 3-D structure with tunable Poisson's ratio and adjustable thermal expansion," *Compos. Commun.*, vol. 22, p. 100431, Dec. 2020, doi: 10.1016/j.coco.2020.100431.

[66] X.-L. Peng and S. Bargmann, "Tunable auxeticity and isotropic negative thermal expansion in three-dimensional lattice structures of cubic symmetry," *Extrem. Mech. Lett.*, vol. 43, p. 101201, Feb. 2021, doi: 10.1016/j.eml.2021.101201.

[67] H. Yazdani Sarvestani, A. H. Akbarzadeh, D. Therriault, and M. Lévesque, "Engineered Bi-material Lattices with Thermo-mechanical Programmability," *Compos. Struct.*, vol. 263, p. 113705, 2021, doi: 10.1016/j.compstruct.2021.113705.

[68] J. Huang, W. Li, M. Chen, and M. Fu, "An Auxetic Material With Negative Coefficient of Thermal Expansion and High Stiffness," *Appl. Compos. Mater.*, pp. 1–26, Nov. 2021, doi: 10.1007/S10443-021-09983-Y/FIGURES/23.

[69] J. Li, Q. Yang, N. Huang, and R. Tao, "A novel mechanical metamaterial with tailorable Poisson's ratio and thermal expansion based on a chiral torsion unit," *Smart Mater. Struct.*, vol. 30, no. 11, p. 115004, Sep. 2021, doi: 10.1088/1361-665X/AC25C9.

[70] L. Wang *et al.*, "Directional instability-driven strain-dependent 3D auxetic metamaterials," *Int. J. Mech. Sci.*, vol. 199, p. 106408, Jun. 2021, doi: 10.1016/J.IJMECSCI.2021.106408.

[71] B. Kosic, A. Dragicevic, Z. Jeli, and G. –C Marinescu, "Application of 3D Printing in the Metamaterials Designing," in *Lecture Notes in Networks and Systems*, vol. 90, Springer, 2020, pp. 166–183.

[72] O. A. Mohamed, S. H. Masood, and J. L. Bhowmik, "Optimization of fused deposition modeling process parameters: a review of current research and future prospects," *Adv. Manuf.*, vol. 3, no. 1, pp. 42–53, Mar. 2015, doi: 10.1007/s40436-014-0097-7.

[73] D. Popescu, A. Zapciu, C. Amza, F. Baciu, and R. Marinescu, "FDM process parameters influence over the mechanical properties of polymer specimens: A review," *Polym. Test.*, vol. 69, pp. 157–166, Aug. 2018, doi: 10.1016/j.polymertesting.2018.05.020.

[74] J. Lluch-Cerezo, R. Benavente, M. D. Meseguer, and J. A. García-Manrique, "Effect of a Powder Mould in the Post-Process Thermal Treatment of ABS Parts Manufactured with FDM Technology," *Polym. 2021, Vol. 13, Page 2422*, vol. 13, no. 15, p. 2422, Jul. 2021, doi: 10.3390/POLYM13152422.

[75] K. Wei, X. Xiao, J. Chen, Y. Wu, M. Li, and Z. Wang, "Additively manufactured bi-material metamaterial to program a wide range of thermal expansion," *Mater. Des.*, vol. 198, p. 109343, Jan. 2021, doi: 10.1016/J.MATDES.2020.109343.

[76] A. Sapienza, V. Brancato, Y. Aristov, and S. Vasta, "Plastic heat exchangers for adsorption cooling: Thermodynamic and dynamic performance," *Appl. Therm. Eng.*, vol. 188, p. 116622, Apr. 2021, doi: 10.1016/J.APPLTHERMALENG.2021.116622.

[77] M. Saviano, R. P. Aquino, P. Del Gaudio, F. Sansone, and P. Russo, "Poly(vinyl alcohol) 3D printed tablets: The effect of polymer particle size on drug loading and process efficiency," *Int. J. Pharm.*, vol. 561, pp. 1–8, Apr. 2019, doi: 10.1016/J.IJPHARM.2019.02.025.

[78] I. Marcelino, "Additive Fabrication of Anepectic Meshes controlled by a NiTi alloy," FCT-NOVA, 2019.

[79] Y. Li, Y. Wan, Y. Shen, X. Lu, and Y. Meng, "Experimental demonstration of lightweight lattice metamaterials with controllable low thermal expansion," *Thin-Walled Struct.*, vol. 159, p. 107112, Feb. 2021, doi: 10.1016/J.TWS.2020.107112.

A

ALGORITHM TO DETERMINE PR

The first step of the algorithm is obtaining the data from the mechanical test, determining the area, calculating the strain and stress, and showing the graphs stress-strain and stress-stroke (until line 77 of algorithm). Then it obtains the video; asks what the maximum relative displacement and the step is; detect each red dot of the corresponded frame; determines the distance in pixel between the dots for each relative displacement and calculates the corresponding average strain (until line 236 of algorithm).

If the program detects more or fewer dots than expected, it will show the images in Figure A.1. The image on the left shows a black and white image of what the algorithm detects as red. The right image is the original frame, where a blue rectangle surrounds the red dots, and a green pixel is put in the considered centre of each red dot.

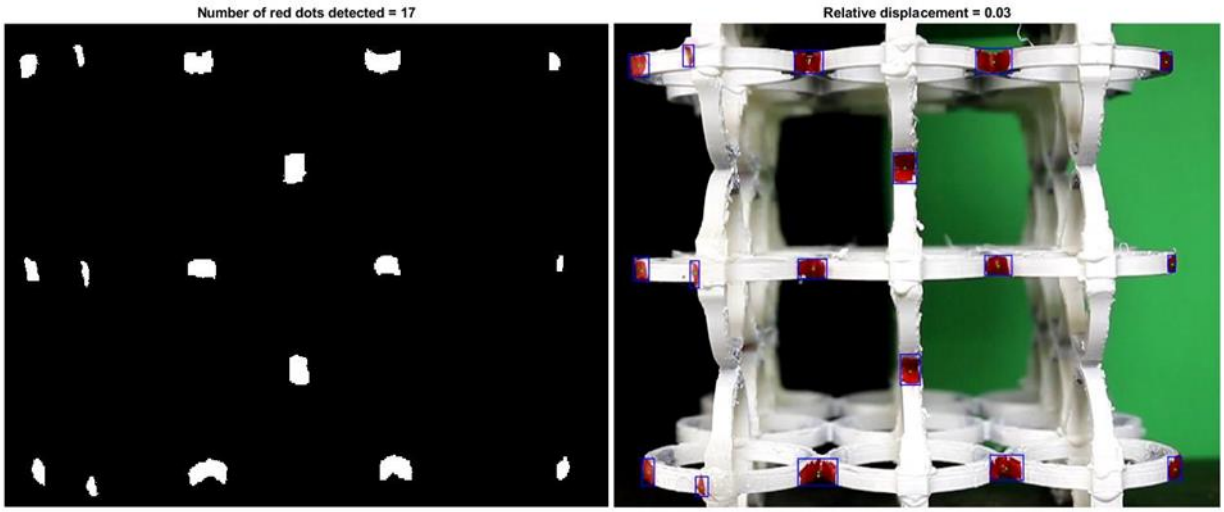

Figure A.1 - Figure shown by the algorithm so the user can see what the algorithm considers a red dot.

After that, calculate the PR of each relative displacement, shows the graphs distance vs relative displacement, strain vs relative displacement, and PR vs relative displacement. Lastly, it saves all data and graphics.

For the algorithm to be functional, it may be necessary to adjust the mask, that is, adjust the values of line 163. Another possible error is the dimension of the points intended to be discarded is not correct. For this case, line 174 is changed.

Below is the code and the detailed explanation (in green) of the algorithm used to determine the PR.

```
1   clear all
2   close all
3
4   fig = 1;
5   %% Open of document with mechanical results
6   fid = fopen('Document_name.txt');
7   tline = fgetl(fid);
8   tlines = cell(0,1);
9   num_line = 0;
10
11  %% Asks for the volume of the structure
12  prompt_1 = {'Volume (mm^3):'};
13  dlgtitle_1 = 'Volume of structure';
14  dims = [1 35];
15  definput_1 = {'32991.9'};
16  answer_1 = inputdlg(prompt_1,dlgtitle_1,dims,definput_1);
17  volume = str2double(answer_1{1});
18
19  time_data = [];
20  force_data = [];
21  stroke_data = [];
22  strain_z_data = [];
23  stress_data = [];
24
25  %%Asks from what stroke does the test starts
26  prompt_2 = {'Conpensated stroke (mm):'};
27  dlgtitle_2 = 'Shift data';
28  definput_2 = {'1.914'};
29  answer_2 = inputdlg(prompt_2,dlgtitle_2,dims,definput_2);
30  stroke_shift = str2double(answer_2{1});
31
32  %%Get the data from the file and calculate stress and strain for each
    point
```

```
33  while ischar(tline)
34      num_line = num_line + 1;
35      if num_line == 11
36          tlines{end+1,1} = tline;
37          slipt_line = split(tlines{end});
38          %% Distances of the structure, measured with a capiler
39          dist_x = str2double(replace(slipt_line{5} ,",",".")); %mm
40          dist_y = str2double(replace(slipt_line{6} ,",",".")); %mm
41          dist_z = str2double(replace(slipt_line{7} ,",",".")); %mm
42          %% Method to determine the area for the calculous of the
    stress
43          volume_ap = dist_x * dist_y * dist_z; %mm^3
44          area_ap = dist_x * dist_y; %mm^2
45          area = (volume / volume_ap) * area_ap; %mm^2
46      elseif num_line > 21
47          tlines{end+1,1} = tline;
48          slipt_line = split(tlines{end});
49          real_time = str2double(replace(slipt_line{1} ,",","."));
50          force = str2double(replace(slipt_line{2} ,",","."));
51          stroke = str2double(replace(slipt_line{3} ,",",".")) -
    stroke_shift;
52          if stroke >= 0
53              time_data(end + 1) = real_time; %seconds
54              force_data(end + 1) = force * 1000; %Newton
55              stroke_data(end + 1) = stroke; %mm
56              strain_z_data(end + 1) = stroke/dist_z;
57              stress_data(end + 1) = (force * 10^3)/(area * 10^-6); %Pa
    (N/m^2)
58          end
59      End
60      tline = fgetl(fid);
61  End
62  fclose(fid);
63
64  %% Shows the graphs Stress vs Strain and Stress vs Stroke
65  figure(fig)
66  plot(strain_z_data, stress_data)
67  title('Stress vs Strain')
68  xlabel('Strain z')
69  ylabel('Stress (Pa)')
70  fig = fig + 1;
71
72  figure(fig)
73  plot(stroke_data, stress_data)
```

```
74  title('Stress vs stroke')
75  xlabel('Stroke')
76  ylabel('Stress (Pa)')
77  fig = fig + 1;
78
79  %%Obtain the video and save in vid
80  vid=VideoReader('Path_of_video\video_name.mp4');
81
82  %% Ask what is the maximum strain and the step which it determine the
    PR
83  prompt_3 = {'Maximum:','Step:'};
84  dlgtitle_3 = 'Video strains';
85  definput_3 = {'0.08','0.01'};
86  answer_3 = inputdlg(prompt_3,dlgtitle_3,dims,definput_3);
87  maximum_strain = str2double(answer_3{1});
88  step = str2double(answer_3{2});
89
90  strain_video = 0 : step : maximum_strain;
91
92  %% Makes vector with zeros to make the code more efficient
93  all_distance_y_central_cell = zeros(1,length(strain_video));
94  strain_y_central_cell = zeros(1,length(strain_video));
95  all_distance_z_central_cell = zeros(1,length(strain_video));
96  strain_z_central_cell = zeros(1,length(strain_video));
97
98
99  all_distance_y_structure = zeros(1,length(strain_video));
100 strain_y_structure = zeros(1,length(strain_video));
101 all_distance_z_structure = zeros(1,length(strain_video));
102 strain_z_structure = zeros(1,length(strain_video));
103
104 %% Ask what time in the video starts the test to compensate with the
    time of the mechanical machine
105 prompt_4 = {'Extra time (s):'};
106 dlgtitle_4 = 'Extra time';
107 definput_4 = {'4'};
108 answer_4 = inputdlg(prompt_4,dlgtitle_4,dims,definput_4);
109 extra_time = str2double(answer_4{1});
110
111 %% This "for" calculate the distance between points and the
    respectively strain
112 for s = 1:length(strain_video)
113     %% Find the index in vector strain_z_data (strain of the machine)
    that has the strain that we want to analise
114     index_resolution = 1e-6;
```

```
115     index = find(abs(strain_z_data - strain_video(s)) <
index_resolution);
116     if isempty(index)
117         while isempty(index)
118             index_resolution = index_resolution + 1e-6;
119             index = find(abs(strain_z_data - strain_video(s)) <
index_resolution);
120         end
121     elseif length(index) > 3
122         while length(index) > 3
123             index_resolution = index_resolution - 1e-6;
124             index = find(abs(strain_z_data - strain_video(s)) <
index_resolution);
125         end
126     end
127     %% obtained the time of the video that has the strain of the
machine we want to analise and obtained the respective frame
128     vid.CurrentTime = time_data(index(round(length(index)/2))) +
extra_time;
129     ImS = readFrame(vid);
130
131     %% If is the initial of the experiment ask if knows all the
necessary data. If not, shows the first frame to obtained the
necessary data.
132     if s == 1
133         pergunta1 = questdlg('Do you know all the initial data?',
'Question 1');
134         if strcmp(pergunta1,'No')
135             figure(fig)
136             imshow(ImS)
137             return
138         end
139         %% If knows the data, asks coordinates to crop the frame to
the necessary size to avoid errors
140         prompt_6 = {'Minimum x:','Maximum x:','Minimum y:','Maximum
y:'};
141         dlgtitle_6 = 'Crop image';
142         definput_6 = {'34' , '1026' , '731' , '1500'};
143         answer_6 = inputdlg(prompt_6,dlgtitle_6,dims,definput_6);
144         Minimum_x = str2double(answer_6{1});
145         Maximum_x = str2double(answer_6{2});
146         Minimum_y = str2double(answer_6{3});
147         Maximum_y = str2double(answer_6{4});
148     end
149
150     %% Crops the frame
151     ImS = ImS(Minimum_y:Maximum_y, Minimum_x:Maximum_x, :);
152
```

```
153     %% Divides the pixels in the red, green and blue part (numbers
        can be from 0 to 255)
154     I_Red = ImS(:,:,1);
155     I_Green = ImS(:,:,2);
156     I_Blue = ImS(:,:,3);
157
158     %% Create an black and white image that put white only if shows
        the correspond conditions.
159     %% These conditions are to put in white only the red pixels.
160     %% There are two different ways to do it, as shown below.
161     %% Then fills holes in the mask.
162     %mask = ((I_Red >= 175 & I_Green <= 210 & I_Blue <= 220) &
        (abs(I_Red - I_Green) > 60) & (abs(I_Red - I_Blue) > 60)) | (I_Red >=
        120 & I_Green <= 100 & I_Blue <= 100) | (I_Red >= 95 & I_Green <= 40
        & I_Blue <= 40) | (I_Red >= 59 & I_Green <= 40 & I_Blue <= 40);
163     mask = (I_Red - I_Green) > 40 & (I_Red - I_Blue) > 40 &
        (abs(I_Green - I_Blue) < 15);
164     mask = imfill(mask, 'holes');
165
166     %% Get the central position of every dot
167     positions_centroid = regionprops(mask,'centroid');
168
169     %% Get the coordinations, and the height and with of the dots
170     positions = regionprops(mask,'BoundingBox');
171
172     %% Eliminate small dots. In other words, remove false dots
173     for i = length(positions):-1:1
174         if  positions(i).BoundingBox(3) * positions(i).BoundingBox(4)
            < 250
175             positions(i) = [];
176             positions_centroid(i) = [];
177         end
178     end
179
180     num_shape = length(positions); % Number of dots
181
182     %% If the number of dots is not the expectec shows the frame to
        visualy try to understand the error.
183     if num_shape ~= 16
184         figure(fig)
185         subplot(1,2,1), imshow(mask);
186         title(num2str(num_shape));
187         subplot(1,2,2), imshow(ImS);
188         for k = 1 : length(positions)
189             all_positions = positions(k).BoundingBox;
```

```
            rectangle('Position', [all_positions(1),
all_positions(2), all_positions(3),
all_positions(4)],'EdgeColor','b','LineWidth',1 )
            rectangle('Position',
[round(positions_centroid(k).Centroid(1)),
round(positions_centroid(k).Centroid(2)),1,1],'EdgeColor','g',
'LineWidth',1)
        end
        title(['strain = ',num2str(strain_video(s))]);
        fig = fig + 1;
    end

    T = struct2table(positions_centroid); % convert the struct array
to a table
    Table = T.Centroid;
    Table = sortrows(Table,2); % sort the table by second collum (by
the height)
    %% Divide and sort by width each line of dots
    Table_Line_1 = sortrows(Table(1:5,:),1);
    Table_Line_2 = sortrows(Table(6,:),1);
    Table_Line_3 = sortrows(Table(7:11,:),1);
    Table_Line_4 = sortrows(Table(12,:),1);
    Table_Line_5 = sortrows(Table(13:end,:),1);

    %%calculation of y strain of central cell
    distance_y_central_cell = Table_Line_3(3,1) - Table_Line_3(2,1);
    all_distance_y_central_cell(s) = distance_y_central_cell;
    strain_y_central_cell(s) = (distance_y_central_cell-
all_distance_y_central_cell(1))/all_distance_y_central_cell(1);

    %%calculation of z strain of central cell
    distance_z_central_cell = Table_Line_4(1,2) - Table_Line_2(1,2);
    all_distance_z_central_cell(s) = distance_z_central_cell;
    strain_z_central_cell(s) = (distance_z_central_cell-
all_distance_z_central_cell(1))/all_distance_z_central_cell(1);

    %%calculation of y strain of structure

    distance_y_structure_1 = Table_Line_1(5,1) - Table_Line_1(1,1);
    distance_y_structure_2 = Table_Line_3(5,1) - Table_Line_3(1,1);
    distance_y_structure_3 = Table_Line_5(5,1) - Table_Line_5(1,1);
    average_distance_y_structure = mean([distance_y_structure_1
distance_y_structure_2 distance_y_structure_3]);
    all_distance_y_structure(s) = average_distance_y_structure;
    strain_y_structure(s) = (average_distance_y_structure-
all_distance_y_structure(1))/all_distance_y_structure(1);

    %%calculation of z strain of structure
```

```
227
228         distance_z_structure_1 = Table_Line_5(1,2) - Table_Line_1(1,2);
229         distance_z_structure_2 = Table_Line_5(2,2) - Table_Line_1(2,2);
230         distance_z_structure_3 = Table_Line_5(3,2) - Table_Line_1(3,2);
231         distance_z_structure_4 = Table_Line_5(4,2) - Table_Line_1(4,2);
232         average_distance_z_structure = mean([distance_z_structure_1
    distance_z_structure_2 distance_z_structure_3
    distance_z_structure_4]);
233         all_distance_z_structure(s) = average_distance_z_structure;
234         strain_z_structure(s) = (average_distance_z_structure -
    all_distance_z_structure(1)) /all_distance_z_structure(1);
235
236     end
237
238     %%calculation of PR of central cell
239     Poisson_z_y_cell = - strain_y_central_cell(2:end) ./
    strain_z_central_cell(2:end);
240     for i = 1:length(Poisson_z_y_cell)
241         if Poisson_z_y_cell(i) == -Inf || Poisson_z_y_cell(i) == 0 ||
    Poisson_z_y_cell(i) == Inf || isnan(Poisson_z_y_cell(i))
242             Poisson_z_y_cell(i) = 0;
243         end
244     end
245
246     %%calculation of PR of structure
247     Poisson_z_y_structure = - strain_y_structure(2:end) ./
    strain_z_structure(2:end);
248     for k = 1:length(Poisson_z_y_structure)
249         if Poisson_z_y_structure(k) == -Inf || Poisson_z_y_structure(k)
    == 0 || Poisson_z_y_structure(k) == Inf ||
    isnan(Poisson_z_y_structure(k))
250             Poisson_z_y_structure(k) = 0;
251         end
252     end
253
254     %%Central cell grafs
255
256     figure_1 = figure(fig);
257     plot(strain_video,all_distance_y_central_cell)
258     hold on
259     plot(strain_video,all_distance_z_central_cell)
260     hold off
261     title('Distance y e z between red dots in central cell vs strain')
262     xlabel('Strain')
263     ylabel('Distance (pixel)')
264     legend('y','z')
```

```
265    fig = fig + 1;
266
267    figure_2 = figure(fig);
268    plot(strain_video,strain_y_central_cell)
269    hold on
270    plot(strain_video,strain_z_central_cell)
271    hold off
272    title('Strain y e z between red dots in central cell vs strain')
273    xlabel('Strain da maquina')
274    ylabel('Strain')
275    legend('y','z')
276    fig = fig + 1;
277
278    figure_3 = figure(fig);
279    plot(strain_video(2:end),Poisson_z_y_cell)
280    title('Poisson_z,y of central cell vs strain')
281    xlabel('Strain')
282    ylabel('Poisson')
283    fig = fig + 1;
284
285    figure_4 = figure(fig);
286    plot(strain_z_central_cell(2:end),strain_y_central_cell(2:end))
287    title('Strain z vs strain y')
288    xlabel('Strain z')
289    ylabel('Strain y')
290    fig = fig + 1;
291
292    %% Structure grafs
293
294    figure_5 = figure(fig);
295    plot(strain_video,all_distance_y_structure)
296    hold on
297    plot(strain_video,all_distance_z_structure)
298    hold off
299    title('Distance y e z between red dots in structure vs strain')
300    xlabel('Strain')
301    ylabel('Distance (pixeis)')
302    legend('y','z')
303    fig = fig + 1;
304
305    figure_6 = figure(fig);
306    plot(strain_video,all_distance_y_structure)
307    hold on
```

```
plot(strain_video,all_distance_z_structure)
hold off
title('Strain y e z between red dots in structure vs strain')
xlabel('Strain da maquina')
ylabel('Strain')
legend('y','z')
fig = fig + 1;

figure_7 = figure(fig);
plot(strain_video(2:end),Poisson_z_y_structure)
title('Poisson_z,y of structure vs strain')
xlabel('Strain')
ylabel('Poisson')
legend('line 1','line 2','line 3')
fig = fig + 1;

figure_8 = figure(fig);
plot(strain_z_structure(2:end),strain_y_structure(2:end))
title('Strain y vs Straun z')
xlabel('Strain z')
ylabel('Strain y')
fig = fig + 1;

%%Ask if want to save the data
question_save_1 = questdlg('Do you want record data?','Question 2');
if strcmp(question_save_1,'No')
    return
end

%%Save the data in an excel
Final_data_1 = num2cell([time_data.' force_data.' stroke_data.'
strain_z_data.' stress_data.']);
header_1 = {'Time (s)','Force (N)','Stroke (mm)','Strain', 'Stress
(Pa)'};
output_matrix_1=[header_1; Final_data_1];

xlswrite('3por3_modelo2_amostra1.xls',output_matrix_1,
'Compressao_y','A1');

Final_data_2 = num2cell([dist_x dist_y dist_z area volume
stroke_shift]);
header_2 = {'Distance x (mm)','Distance y (mm)','Distance z
(mm)','Area', 'Sample volume', 'Stroke shift (mm)'};
output_matrix_2=[header_2; Final_data_2];

```

```
xlswrite('3por3_modelo2_amostra1.xls',output_matrix_2,
'Compressao_y','G1');

Final_data_vista_y = num2cell([strain_video.'
all_distance_y_central_cell.' all_distance_z_central_cell.'
strain_y_central_cell.' strain_z_central_cell.'
all_distance_y_structure.' all_distance_z_structure.'
strain_y_structure.' strain_z_structure.']);
header_poisson_y = {'Strain','Distance cell y (pixels)', 'Distance
cell z (pixels)', 'Strain cell y' ,'Strain cell z', 'Distance y
stuture (pixel)', 'Distance z stuture (pixel)', 'Strain y stuture',
'Strain z stuture'};
output_matrix_vista_y = [header_poisson_y; Final_data_vista_y];

xlswrite('3por3_modelo2_amostra1.xls',output_matrix_vista_y,'vista_y'
);

Final_data_vista_y_2 = num2cell([Poisson_z_y_cell.'
strain_video(2:end).' Poisson_z_y_structure.']);
header_3 = {'Poisson_z_y cell', 'Strain video', 'Poisson_z_y
structure'};
output_matrix_vista_y_2=[header_3; Final_data_vista_y_2];

xlswrite('3por3_modelo2_amostra1.xls',output_matrix_vista_y_2,'vista_
y','L1');

%% Ask if want to save graphs
question_save_2 = questdlg('Pretende guardar graficos?','Pergunta
3');
if strcmp(question_save_2,'No')
    return
end

%% Save the graphs
saveas(figure_1,'central_cell_distance_y_z.png')
saveas(figure_2,'central_cell_strain_y_z.png')
saveas(figure_3,'central_cell_poisson_z_y.png')
saveas(figure_4,'central_cell_declive_y_z.png')

saveas(figure_5,'structure_distance_y_z.png')
saveas(figure_6,'structure_strain_y_z.png')
saveas(figure_7,'structure_poisson_z_y.png')
saveas(figure_8,'structure_declive_y_z.png')
```

B

Algorithm to determine CTE

The first step of the algorithm is obtaining the images. After that, detects each red dot of the corresponded image; determines the distance in pixel between the dots center for each image and calculates the corresponding CLTE (until line 133).

For each image, it will show the images in Figure B.1. The image on the left shows a black and white image of what the algorithm detects as red. The right image is the original image, where a blue rectangle surrounds the red dots, and a blue pixel is put in the considered centre of each red dot that needs to determine all the distances.

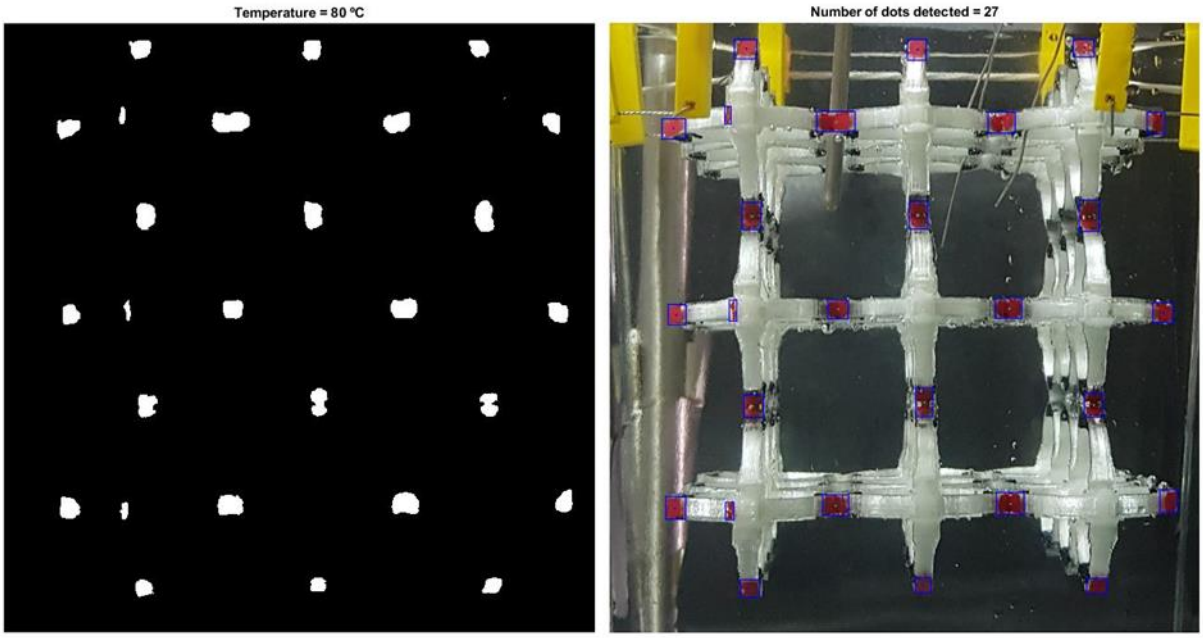

Figure B.1 - Figure shown by the algorithm so the user can see what the algorithm considers a red dot and what is the centre of each dot.

After that, shows the graphs distance vs temperature and CLTE vs temperature. Lastly, it saves all data and graphics.

Below is the code and the detailed explanation of the algorithm used to determine the CLTE.

```
1   clear all
2   close all
3
4   %Get the images
5   files = dir('*.jpg');
6
7   %Vector of all the temperature study
8   Temperature = [21 30 40 50 60 70 80];
9
10  % Makes vector with zeros to make the code more efficient
11  all_distance_x_estrutura = zeros(1,length(files));
12  all_distance_z_estrutura = zeros(1,length(files));
13  expansion_x = zeros(1,length(files));
14  expansion_z = zeros(1,length(files));
15  fig = 1;
16
17  % This "for" calculate the distance between points and the
    respectively CLTE
18  for j = 1:length(files)
19      I = imread(files(j).name);
20      I = imrotate(I,-90);
21
22      % If is the initial of the experiment ask if knows all the
    necessary data.
23      % If not, shows the first frame to obtained the necessary data.
24      if j == 1
25          pergunta1 = questdlg('Quer só a primeira imagem?','Pergunta
    1');
26          if strcmp(pergunta1,'Yes')
27              figure(fig)
28              imshow(I)
29              Return
30          End
31      End
32
33      % If knows the data, asks coordinates to crop the frame to the
    necessary size to avoid errors
34      prompt = {'Minimum x:','Maximum x:','Minimum y:','Maximum y:'};
35      dlgtitle = 'Crop image';
```

```
36      definput = {'34' , '1026' , '731' , '1500'};
37      answer = inputdlg(prompt,dlgtitle,dims,definput);
38      Minimum_x = str2double(answer{1});
39      Maximum_x = str2double(answer{2});
40      Minimum_y = str2double(answer{3});
41      Maximum_y = str2double(answer{4});
42
43      % Crops the frame
44      I = I(Minimum_y:Maximum_y, Minimum_x:Maximum_x, :);
45
46      % Divides the pixels in the red, green and blue part (numbers
    can be from 0 to 255)
47      I_Red = I(:,:,1);
48      I_Green = I(:,:,2);
49      I_Blue = I(:,:,3);
50
51      % Create a black and white image that put white only if shows
    the correspond conditions.
52      % These conditions are to put in white only the red pixels.
53      mask = (I_Red - I_Green) > 30 & (I_Red - I_Blue) > 30 &
    (abs(I_Green - I_Blue) < 20);
54
55      % Then fills holes in the mask.
56      mask = imfill(mask, 'holes');
57
58      % Get the central position of every dot
59      positions_centroid = regionprops(mask,'centroid');
60
61      % Get the coordinations, and the height and with of the dots
62      positions = regionprops(mask,'BoundingBox');
63
64      % Eliminate small dots. In other words, remove false dots
65      for i = length(positions):-1:1
66          if  positions(i).BoundingBox(3) *
    positions(i).BoundingBox(4) < 250
67              positions(i) = [];
68              positions_centroid(i) = [];
69          End
70      end
71
72      num_shape = length(positions); % Number of dots
73
74      % Shows the image and the mask to visualy understand if
    everything is well.
75      figure(fig)
```

```
76      subplot(1,2,1), imshow(mask);
77      title(num2str(j));
78      subplot(1,2,2), imshow(I);
79      title(num2str(num_shape));
80      for k = 1 : length(positions)
81         all_positions = positions(k).BoundingBox;
82         rectangle('Position', [all_positions(1), all_positions(2)
    ,all_positions(3) ,all_positions(4)], 'EdgeColor','b','LineWidth',1
    )
83         rectangle('Position',
    [round(positions_centroid(k).Centroid(1)),
    round(positions_centroid(k).Centroid(2)),1,1],'EdgeColor','g','Line
    Width',1)
84      End
85
86      T = struct2table(positions_centroid); % convert the struct
    array to a table
87      Table = T.Centroid;
88      Table = sortrows(Table,2); % sort the table by second collum (z
    direction)
89      % Devide in line and sort in x diretion
90      Table_Line_1 = sortrows(Table(1:3,:),1);
91      Table_Line_2 = sortrows(Table(4:7,:),1);
92      Table_Line_3 = sortrows(Table(8:10,:),1);
93      Table_Line_4 = sortrows(Table(11:14,:),1);
94      Table_Line_5 = sortrows(Table(15:17,:),1);
95      Table_Line_6 = sortrows(Table(18:21,:),1);
96      Table_Line_7 = sortrows(Table(22:24,:),1);
97      % To visually observe where is the center of the dotts
98      rectangle('Position', [round(Table_Line_2(1,1)),
    round(Table_Line_2(1,2)),1,1],'EdgeColor','b','LineWidth',1)
99      rectangle('Position', [round(Table_Line_2(4,1)),
    round(Table_Line_2(4,2)),1,1],'EdgeColor','b','LineWidth',1)
100     rectangle('Position', [round(Table_Line_4(1,1)),
    round(Table_Line_4(1,2)),1,1],'EdgeColor','b','LineWidth',1)
101     rectangle('Position', [round(Table_Line_4(4,1)),
    round(Table_Line_4(4,2)),1,1],'EdgeColor','b','LineWidth',1)
102     rectangle('Position', [round(Table_Line_6(1,1)),
    round(Table_Line_6(1,2)),1,1],'EdgeColor','b','LineWidth',1)
103     rectangle('Position', [round(Table_Line_6(4,1)),
    round(Table_Line_6(4,2)),1,1],'EdgeColor','b','LineWidth',1)
104
105     rectangle('Position', [round(Table_Line_1(1,1)),
    round(Table_Line_1(1,2)),1,1],'EdgeColor','b','LineWidth',1)
106     rectangle('Position', [round(Table_Line_1(2,1)),
    round(Table_Line_1(2,2)),1,1],'EdgeColor','b','LineWidth',1)
107     rectangle('Position', [round(Table_Line_1(3,1)),
    round(Table_Line_1(3,2)),1,1],'EdgeColor','b','LineWidth',1)
108     rectangle('Position', [round(Table_Line_7(1,1)),
    round(Table_Line_7(1,2)),1,1],'EdgeColor','b','LineWidth',1)
```

```
109     rectangle('Position', [round(Table_Line_7(2,1)),
    round(Table_Line_7(2,2)),1,1],'EdgeColor','b','LineWidth',1)
110     rectangle('Position', [round(Table_Line_7(3,1)),
    round(Table_Line_7(3,2)),1,1],'EdgeColor','b','LineWidth',1)
111
112
113
114     % calculation of the CLTE in x direction
115
116     distance_x_estrutura_1 = Table_Line_2(4,1) - Table_Line_2(1,1);
117     distance_x_estrutura_2 = Table_Line_4(4,1) - Table_Line_4(1,1);
118     distance_x_estrutura_3 = Table_Line_6(4,1) - Table_Line_6(1,1);
119     average_distance_x_estrutura = mean([distance_x_estrutura_1
    distance_x_estrutura_2 distance_x_estrutura_3]);
120     all_distance_x_estrutura(j)= average_distance_x_estrutura;
121     expansion_x(j) = ((average_distance_x_estrutura-
    all_distance_x_estrutura(1))/all_distance_x_estrutura(1)) *
    (1/(Temperature(j)-Temperature(1)));
122
123     % calculation of the CLTE in z direction
124
125     distance_z_estrutura_1 = Table_Line_7(1,2) - Table_Line_1(1,2);
126     distance_z_estrutura_2 = Table_Line_7(2,2) - Table_Line_1(2,2);
127     distance_z_estrutura_3 = Table_Line_7(3,2) - Table_Line_1(3,2);
128     average_distance_z_estrutura = mean([distance_z_estrutura_1
    distance_z_estrutura_2 distance_z_estrutura_3]);
129     all_distance_z_estrutura(j)= average_distance_z_estrutura;
130     expansion_z(j) = ((average_distance_z_estrutura-
    all_distance_z_estrutura(1))/all_distance_z_estrutura(1))*(1/(
    Temperature(j)-Temperature(1)));
131
132     fig = fig + 1;
133 End
134
135 %Grafs to verify the results
136 %Graf 1 : Temperature vs Distances in x and z directions
137 %Graf 2 : Temperature vs CLTE in x and z directions
138
139 figure_1 = figure(fig);
140 plot(Temperature,all_distance_x_estrutura)
141 hold on
142 plot(Temperature,all_distance_z_estrutura)
143 hold off
144 title('Distance')
145 xlabel('Temperature')
146 ylabel('Distance (pixeis)')
```

```
147  legend('x','z')
148
149  fig = fig + 1;
150
151  figure_2 = figure(fig);
152  plot(Temperature(2:end),expansion_x(2:end))
153  hold on
154  plot(Temperature(2:end),expansion_z(2:end))
155  hold off
156  title('CTE')
157  xlabel('Temperature')
158  ylabel('Distance (pixeis)')
159  legend('x','z')
160
161  %Ask if want to save the data
162  question_save_1 = questdlg('Pretende guardar dados?','Pergunta 2');
163  if strcmp(question_save_1,'No')
164      return
165  End
166
167  Final_data_view_x_1 = num2cell([Temperature.'
     all_distance_x_estrutura.']);
168  header_1 = {'Temperature', 'Distance x (pixel)'};
169  output_matrix_view_x_1=[header_1; Final_data_view_x_1];
170
171  xlswrite('3por3_modelo2_amostra2_view_zx.xls',output_matrix_view_x_
     1,'direcao_x');
172
173  Final_data_view_x_2 = num2cell([Temperature(2:end).'
     expansion_x(2:end).']);
174  header_2 = {'Temperature', 'Distance x (pixel)'};
175  output_matrix_view_x_2=[header_2; Final_data_view_x_2];
176
177  xlswrite('3por3_modelo2_amostra2_view_zx.xls',
     output_matrix_view_x_2,'direcao_x','D1');
178
179  Final_data_view_z_1 = num2cell([Temperature.'
     all_distance_z_estrutura.']);
180  header_3 = {'Temperature', 'Distance z (pixel)'};
181  output_matrix_view_z_1=[header_3; Final_data_view_z_1];
182
183  xlswrite('3por3_modelo2_amostra2_view_zx.xls',
     output_matrix_view_z_1,'direcao_z');
184
185  Final_data_view_z_2 = num2cell([Temperature(2:end).'
     expansion_z(2:end).']);
```

```
186  header_4 = {'Temperature', 'Distance z (pixel)'};
187  output_matrix_view_z_2=[header_4; Final_data_view_z_2];
188
189  xlswrite('3por3_modelo2_amostra2_view_zx.xls',
     output_matrix_view_z_2,'direcao_z','D1');
190
191  %Ask if want to save the graphs
192  question_save_2 = questdlg('Do you want to save the
     graphs?','Pergunta 3');
193  if strcmp(question_save_2,'No')
194      Return
195  End
196
197  %Save the graphs
198  saveas(figure_1,'model_2_distance_view_xz.png')
199  saveas(figure_2,'model_2_CTE_view_yz.png')
```

C

STRESS-STRAIN CURVES OF FILAMENTS

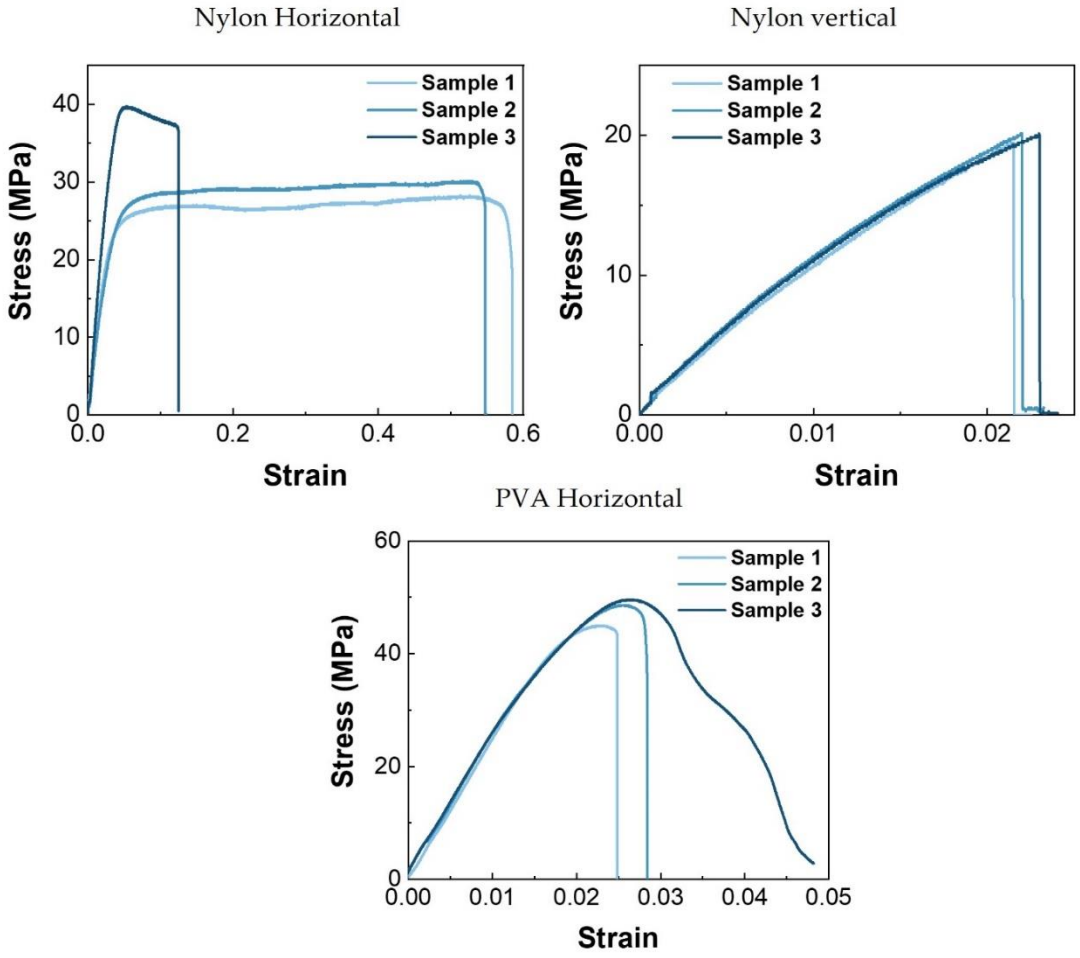

Figure C.1 - Tensile curve of Nylon (horizontal and vertical orientation) and PVA (horizontal orientation).

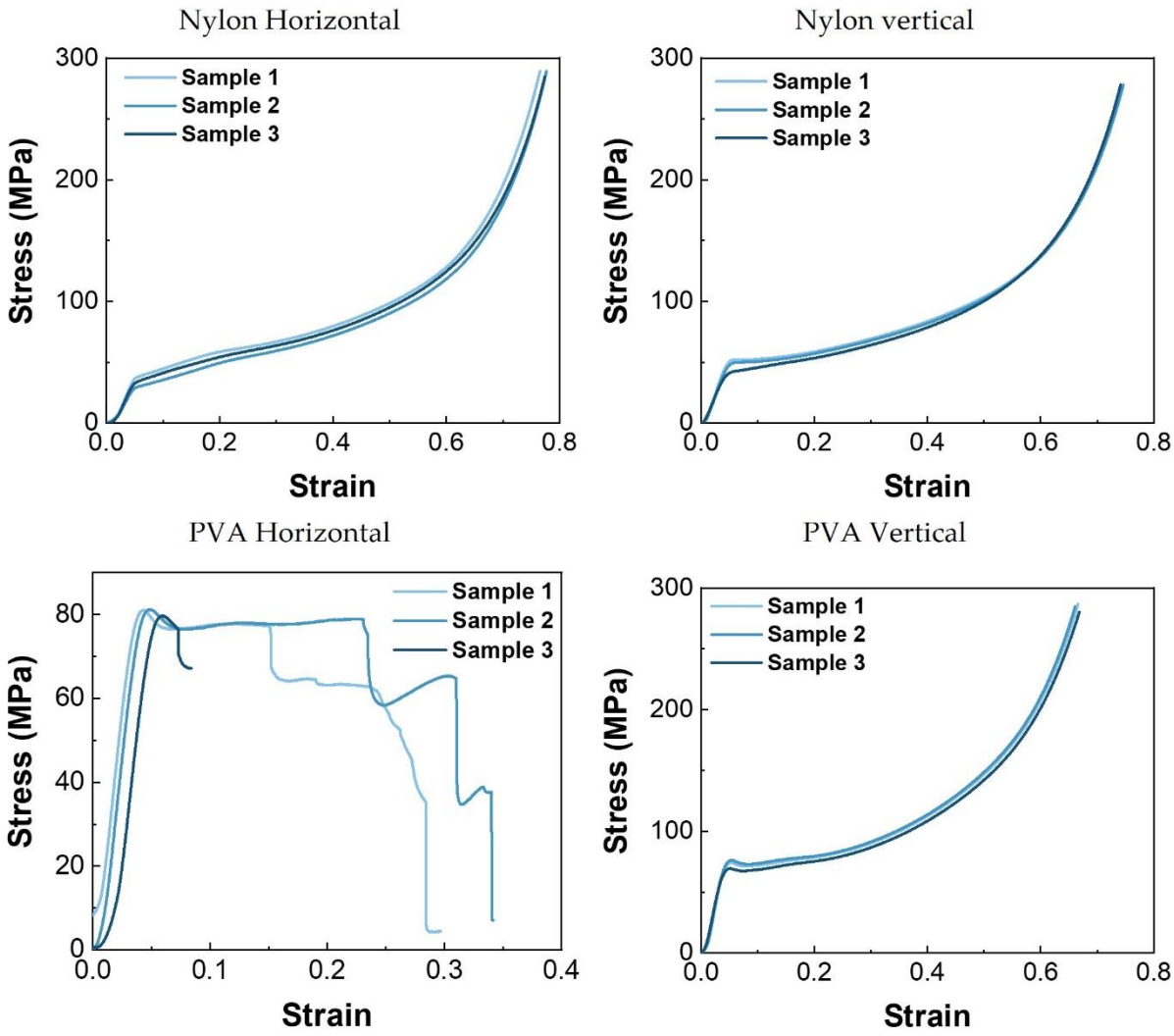

Figure C.2 - Compression curve of Nylon and PVA with the respective printing orientation.

D

DIFFERENT CELL ARRANGEMENTS STUDIED

Figure D.1 displays three of the four cells studied using a FE analysis. After the thermal simulations it was observed that the arrangements a) and b) of Figure D.1 show a positive CTE, while the arrangement c) shows a negative CLTE in one of the directions. The main reason for not continuing the study of this arrangement is because it was observed a negative behaviour in only one direction while in the unit cell chosen (Figure 3.2) it has a negative CLTE in two directions.

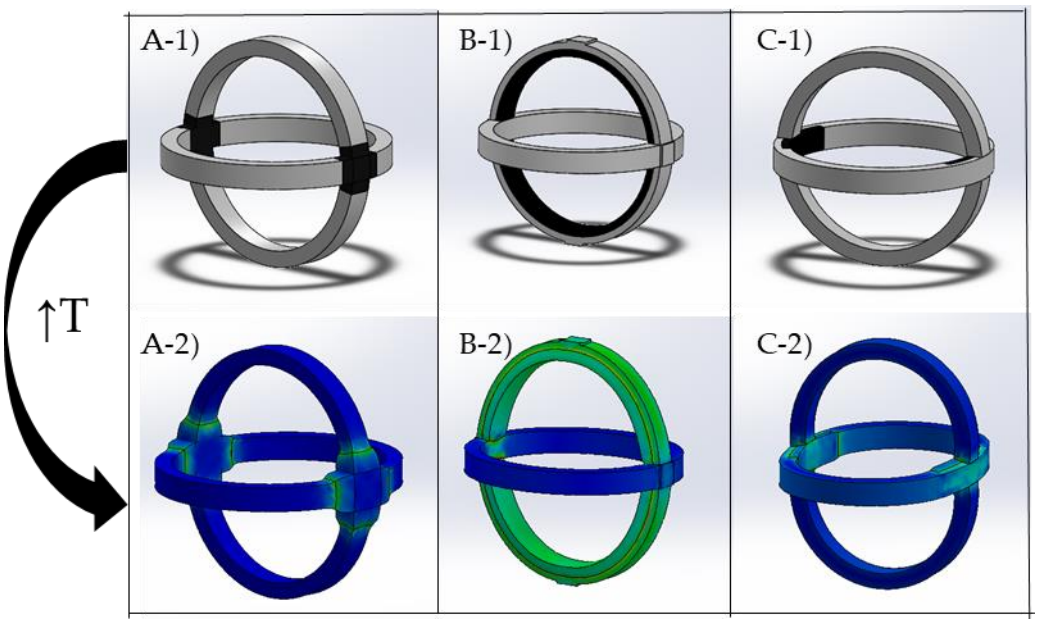

Figure D.1 - Thermal simulation of three different cell arrangements, in white is represented PVA, while in black is Nylon.

E

PRINT ATTEMPTS

Table E-1 - Print attempts summary.

Test	q (mm)	t_0 (mm)	Temperature (ºC)	Velocity (mm/s)	Support	Notes	Results
Unit cell (only PVA)	3	2	215	30	none		broke cell
Unit cell (only PVA)	3	2	215	25	tree support		broke support
Unit cell (only PVA)	3	2	215	25	none		broke cell
Unit cell (only PVA)	3	2	215	25	tree support		broke cell
Unit cell (only PVA)	3	2	215	25	Custom support		broke cell
Unit cell (only PVA)	3	2	220	20	tree support		broke one of rings
Unit cell (only PVA)	5	5	220	20	none		broke one of rings
Unit cell (only PVA)	5	5	220	20	custom support		printed
Unit cell (only PVA)	5	5	220	20	none		broke one of rings
Unit cell (only PVA)	5	5	205	20	none		Broke

Unit cell (only PVA)	5	5	190	20	none		broke one of rings
Unit cell (only PVA)	5	5	190	20	none	infill pattern: concentric	broke one of rings
Ring (only PVA)	10	5	190	20	none	z hop and retraction	printed
Ring (only PVA)	7,5	5	190	20	none	z hop and retraction	printed
Unit cell (only PVA)	10	5	190	20	none	z hop and retraction	broke
Unit cell (only PVA)	10	5	200	20	none	z hop and retraction	printed
Unit cell (only PVA)	7,5	5	200	20	none	z hop and retraction	printed
Unit cell	7,5	5	200 - 240	20 - 30	none	retraction	printed
Unit cell	5	5	200 - 240	20 - 30	none	retraction	broke
Unit cell	5	5	200 - 245	15 - 30	none	retraction	printed
Unit cell	3	2	200 - 245	15 - 30	none	retraction	broke
Unit cell	5	5	200 - 245	15 - 30	none	retraction	broke
Unit cell	5	3	200 - 245	15 - 30	none	retraction	broke
Unit cell	5	5	200 - 245	25 - 30	none	retraction	printed
Unit cell	5	5	200 - 245	30 - 30	none	retraction	printed
3 x 3 x 3 structure	5	5	200 - 245	30 - 30	Outside cell supports	retraction	broke in several cells
3 x 3 x 3 structure	5	5	200 - 245	30 - 30	support on the outside cells	retraction	broke in several cells

All print attempts were made with a 0.15 layer height and 100 % infill.

F

DESIGN OF THE PRINTING PARTS

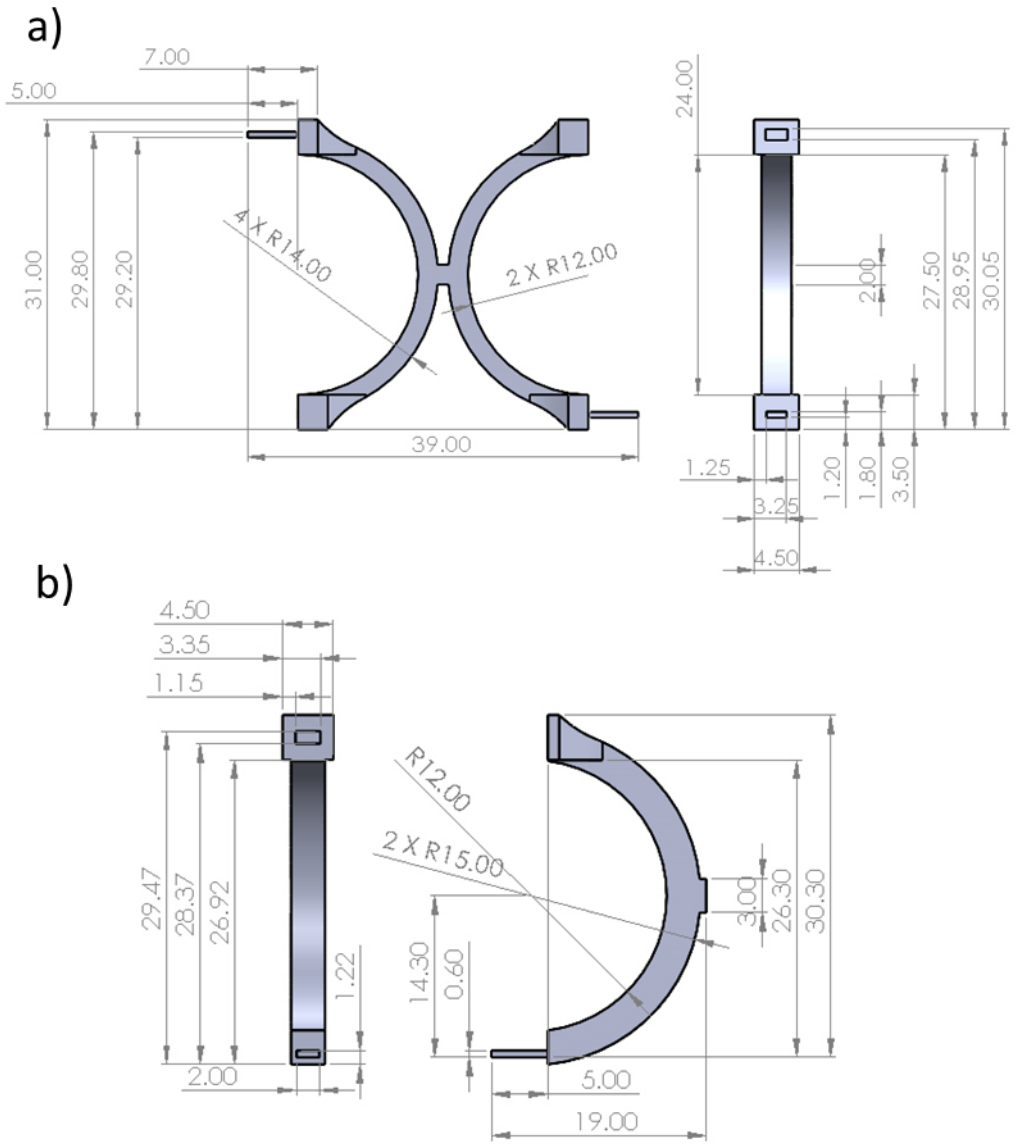

Figure F.1 - Design of the: a) inner connection piece; and b) exterior connection piece.

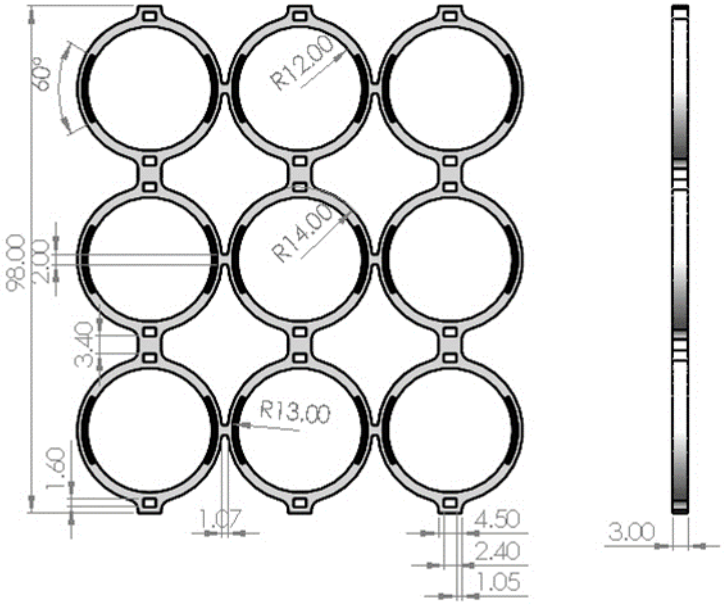

Figure F.2 - Design of the 3 x 3 ring mesh.

Table F-1 indicates the number of pieces necessary to manufacture all the structures used in this work.

Table F-1 - Number of pieces for each structure.

Structure type	Inner connection piece	Exterior connection piece	Ring mesh
Unit cell	0	2	1 (1 ring mesh)
2 x 2 x 2 structure	4	8	2 (2 x 2 ring mesh)
3 x 3 x 3 structure	18	18	3 (3 x 3 ring mesh)

G

UNIT CELLS STRESS-STRAIN CURVES

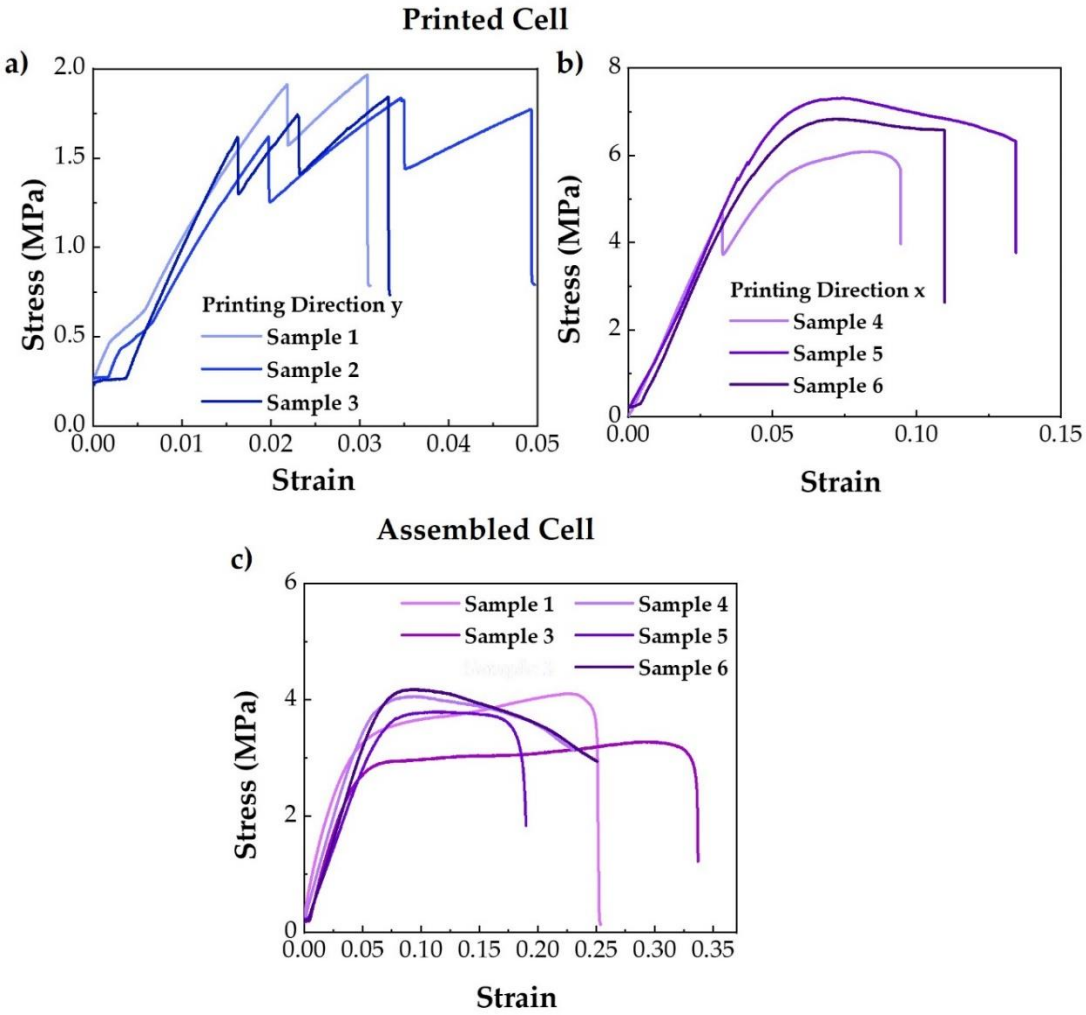

Figure G.1 - Stress-strain curves of unit cell: a) Printed in direction y; b) Printed in direction x; c) Assembled cell.

H

UNIT CELL PR

Figure H.1 shows an example of a compressive test of a unit cell. The red circles indicate the dots used to determine the strain in x and y direction. The relative displacement of the compression cylinder was used as the strain on the z direction.

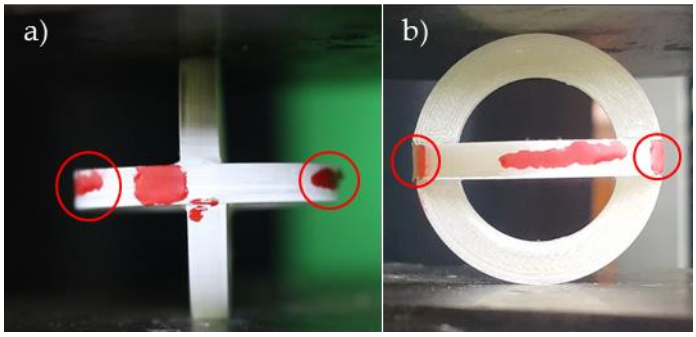

Figure H.1 - Example of a compressive test of a unit cell a) view of the xz plane; b) view of the yz plane.

The figure below indicates the PR of the assembled cells.

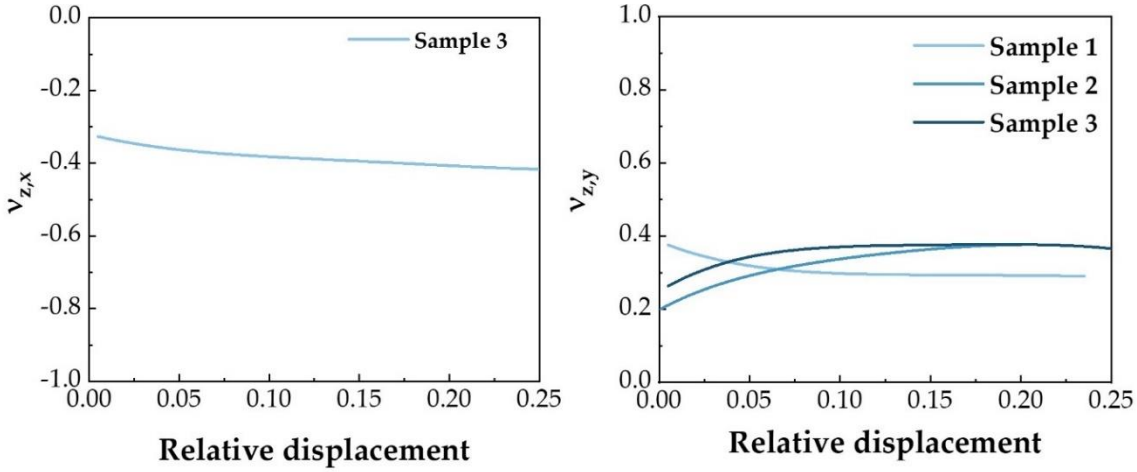

Figure H.2 - PR of the assembled cells.

I

2 x 2 x 2 STRESS-STRAIN CURVES

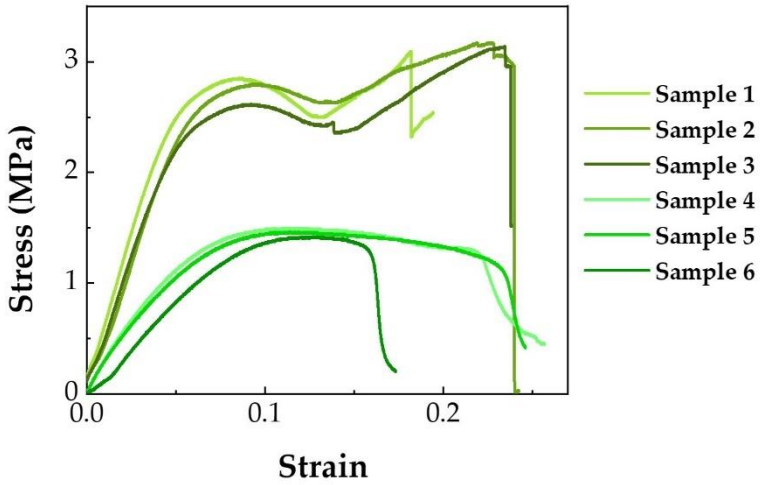

Figure I.1 - Stress-strain curves of 2 x 2 x 2 structure.

J

2 x 2 x 2 PR

Figure J.1 shows an example of a compressive test of a 2 x 2 x 2 structure. The red circles indicate the dots used to determine the strain in x and y direction. The relative displacement of the compression cylinder was used as the strain on the z direction.

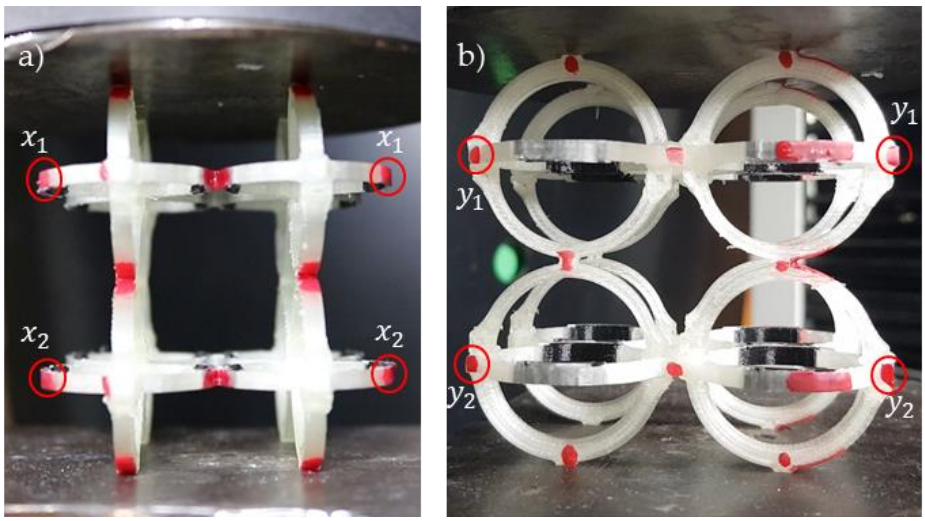

Figure J.1 - Example of a compressive test of a 2 x 2 x 2 structure a) view of the xz plane; b) view of the yz plane.

Figure J.2 shows the PR of the 2 x 2 x 2 structures. It is possible to observe that sample 3 is an outlier. For that reason, it was not accounted for the average calculation of PR.

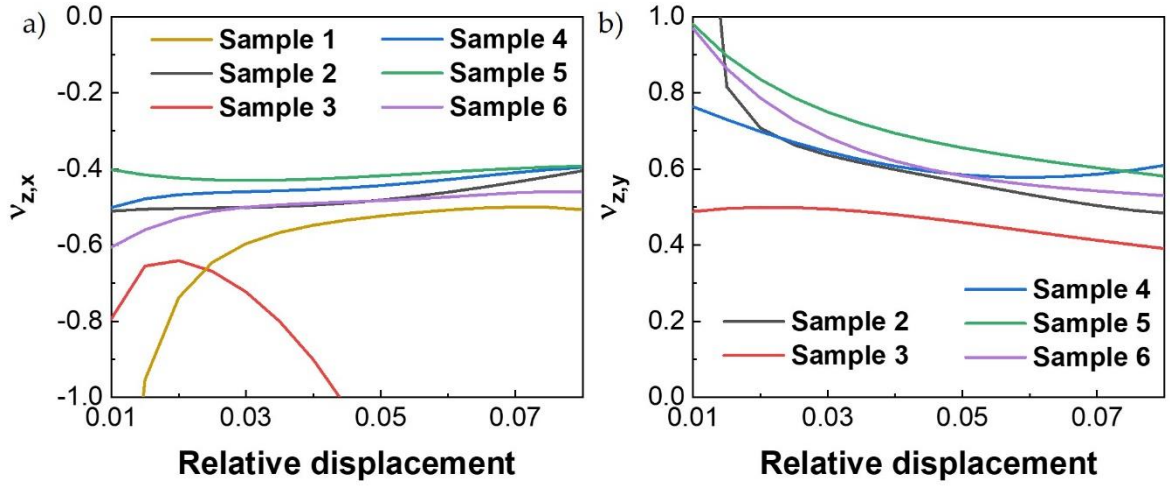

Figure J.2 - PR of the 2 x 2 x 2 structure.

K

3 x 3 x 3 STRESS-STRAIN CURVES

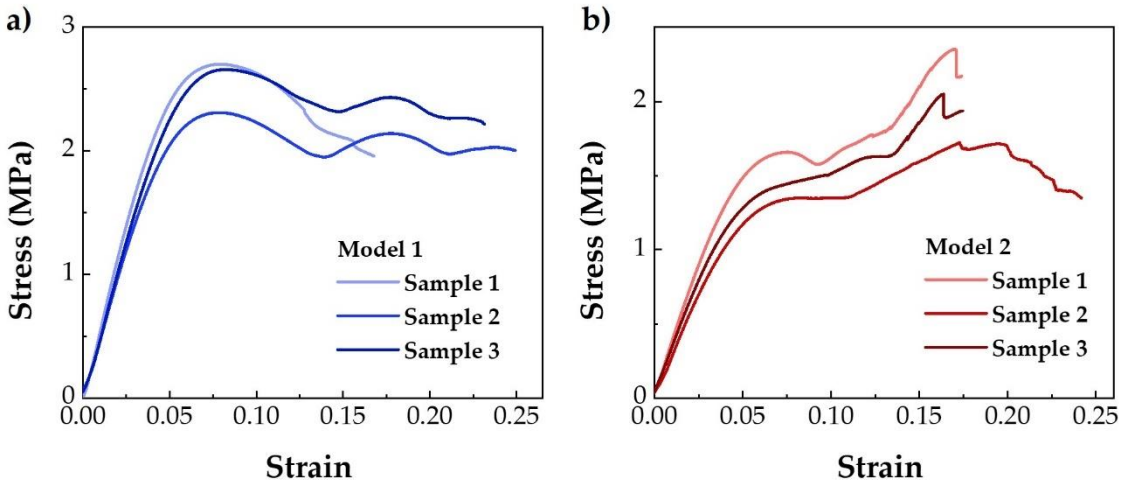

Figure K.1 - Stress-strain curves of 3 x 3 x 3 structure a) model 1; b) model 2.

L

3 x 3 x 3 PR

Figure L.1 shows an example of a compressive test of a 3 x 3 x 3 structure. The blue circles indicate the dots used to determine the strains.

The exterior dots of the samples were used to determine the PR of the structure. For the strain in x and y directions, the distance between points 1 and 4, 6 and 9, and 11 and 14 of Figure L.1 a) and b), respectively, were used. In both views, the distance between dots 1 and 11, 2 and 12, 3 and 13, and 4 and 14 were used to calculate the strain in z direction.

To determine the PR of the central cell it was used the dots 5, 7, 8 and 10 of Figure L.1.

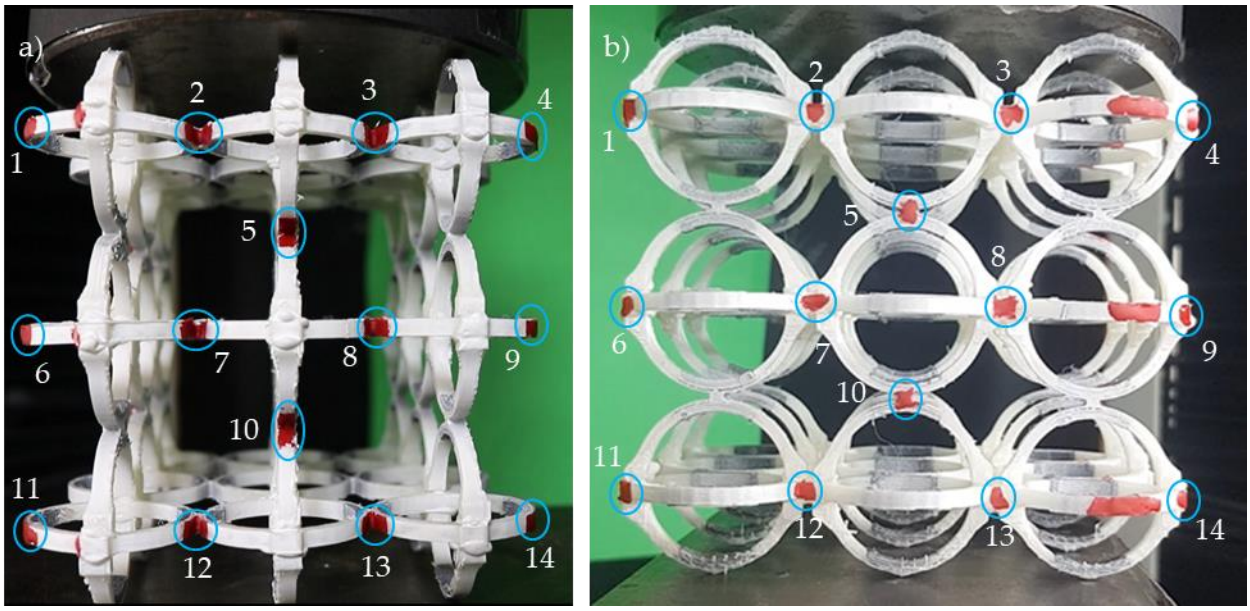

Figure L.1 - Example of a compressive test of a 3 x 3 x 3 structure a) view of the xz plane; b) view of the yz plane.

Figure L.2 shows the PR of the 3 x 3 x 3 structures and central cell of model 1 and model 2. For the calculation of the average PR some samples or zones of the sample were discarded for being outliers.

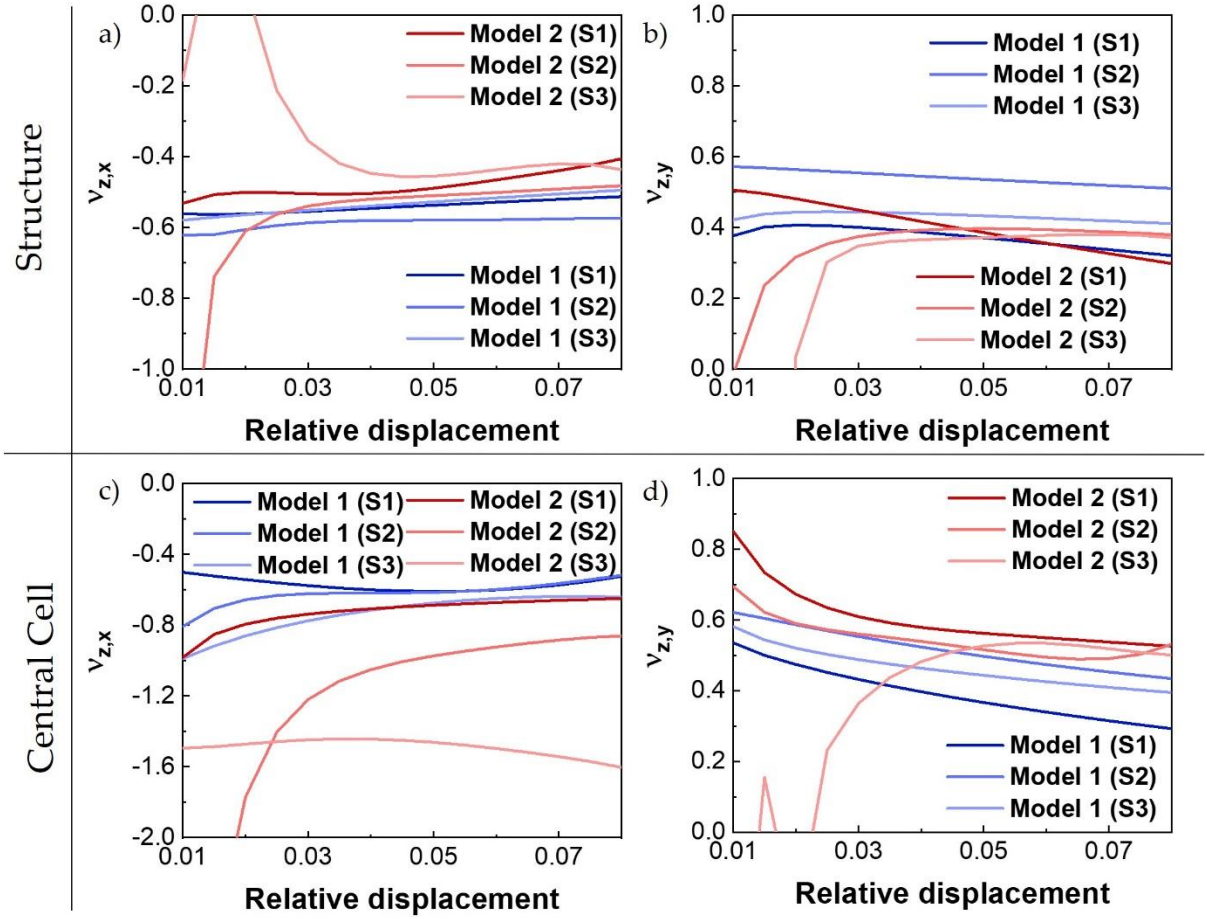

Figure L.2 - PR of the structure and central cell of model 1 and 2

M

CLTE CALCULATION OF 3 X 3 X 3 STRUCTURE

Figure M.1 shows an example of a thermal test of a 3 x 3 x 3 structure. The blue circles indicate the dots used to determine the CLTE. For the determination of CLTE in x and y directions, the distance between points 4 and 5, 6 and 7, and 8 and 9 of Figure M.1 a) and b), respectively, were used. In both views, the distance between dots 1 and 10, 2 and 11, and 3 and 12 were used to calculate the CLTE in z direction.

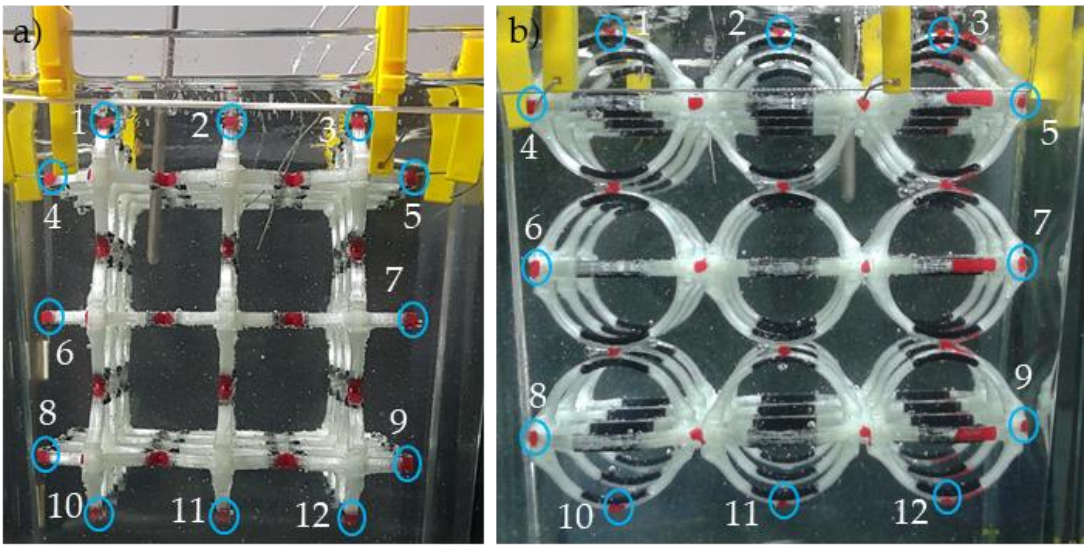

Figure M.1 - Example of a thermal test of a 3 x 3 x 3 structure a) view of the xz plane; b) view of the yz plane.

N

PRINTED HEXAGONAL GEOMETRY STRUCTURE

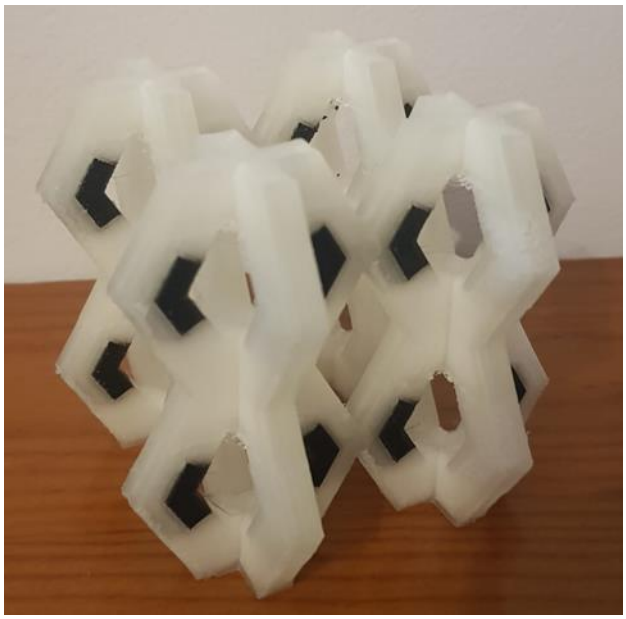

Figure N.1 - A 2 x 2 x 2 hexagonal geometry structure printed at once.